

# Effects of Training Data Quality on Classifier Performance

Alan F. Karr\*

Regina Ruane<sup>†</sup>

February 26, 2026

## Abstract

We describe extensive numerical experiments assessing and quantifying how classifier performance depends on the quality of the training data, a frequently neglected component of the analysis of classifiers.

More specifically, in the scientific context of metagenomic assembly of short DNA reads into “contigs,” we examine the effects of degrading the quality of the training data by multiple mechanisms, and for four classifiers—Bayes classifiers, neural nets, partition models and random forests. We investigate both individual behavior and congruence among the classifiers. We find breakdown-like behavior that holds for all four classifiers, as degradation increases and they move from being mostly correct to only coincidentally correct, because they are wrong in the same way. In the process, a picture of spatial heterogeneity emerges: as the training data move farther from analysis data, classifier decisions degenerate, the boundary becomes less dense, and congruence increases.

## 1 Introduction

As articulated in Porter and Karr (2024), (supervised) classifiers should be construed as software systems with at least three components, the classifier itself, the *training data* on which it draws, and the *analysis data* to which it is applied. When diagnosing problems, all three of these components matter. In this paper, we focus on the training data, which we believe are (too) often neglected, since quality of the training data affect performance on all analysis datasets. While there may be general acknowledgement that classifiers become less trustworthy the more the analysis data depart from the training data, there is little quantification of either “less trustworthy” or “depart from.”

To address this neglect, we conducted and report here an extensive set of numerical experiments with

- A single analysis dataset consisting of short DNA sequences;
- Four classifiers: a Bayes classifier, a neural net, a partition model, and a random forest model;
- A single parent training dataset whose quality is degraded in multiple ways, especially, but not exclusively, using the SNP degradation in Karr et al. (2022).

---

\*Department of Statistics, Operations and Data Science, Temple University, Philadelphia PA 19122 and Fraunhofer USA Center Mid-Atlantic, Riverdale MD 20737; alan.karr@temple.edu

<sup>†</sup>Computational Social Science Laboratory, University of Pennsylvania, Philadelphia, PA 19104; jeanneruane@gmail.com

The experimental results include correctness, Boundary Status (Karr et al., 2026), congruence among the four classifiers, and Neighbor Similarity (Karr et al., 2026).

It is important to understand the restriction to decreased data quality, the detailed rationale for which can be found in Karr et al. (2022). In reality, improving data quality is expensive and often statistically problematic. (Exceptions are imputation and editing in official statistics, for which there is strong theoretical and methodological basis.) By contrast, data quality can readily be decreased, provided that the mechanism is contextually credible, as it is in Karr et al. (2022). Here, we use both it and others that are equally credible.

Finally, we note the important adversarial aspect of data quality degradation. While data quality problems are typically conceived as the result of uncontrollable but benign external forces, they may also result from actions deliberately intended to cause harm, such as attempts to “poison” genomic databases (Farbiash and Puzis, 2020; Porter and Karr, 2024).

## 2 Background and Problem Formulation

This section contains background on data quality, metagenomic assembly, classifiers, and classifier boundaries.

### 2.1 Data Quality

Attention to data quality has waxed and waned over time (Karr et al., 2001, 2006; Keller et al., 2017). Given currently generated volumes of data, data quality effort per data element may be at an all-time low. There are exceptions, of course, especially official statistics, in which the total survey error (TSE) paradigm (Office of Management and Budget, 2002, 2006; Biemer et al., 2017; Karr, 2017) has perpetuated and to some degree codified longstanding attention to data quality. Other than data volume, perhaps the most pressing issues are inability to quantify data quality at any level, from the data point to the dataset, and properly to incorporate data quality as a source of uncertainty in statistical analyses.

Initial investigations in Karr et al. (2022) exploit the ease with which we can decrease (synonymously, “degrade”) data quality in ways that both are plausible scientifically and can be parameterized. This setting appears in Section 4.1. The effects of deliberately decreasing data quality can also be used to characterize and even quantify the quality of individual data points. Across a range of scientific settings, higher quality data points are more “fragile,” and are affected more by the same amount of degradation than low quality data points. This is illustrated graphically in Figure 1. There, 26,964 virus genomes are degraded by successive applications of the `Mason_variator` haplotype generation software (Holtgrewe, 2010). In the figure, there are 26,943 coronavirus genomes in green, previously degraded versions of 10 of these in red, and one adenovirus genome in blue. (For reference, the parents of the 10 degraded genomes in red are in yellow.) The  $x$ -axis is the number of iterations of the `Mason_variator`. The  $y$ -axis is entropy, with the interpretation that higher values mean lower quality.

Evidently, there are “decreasing returns to scale” from increased degradation. The coronavirus genomes fall into several classes with respect to initial entropy, which is argued in Karr et al. (2023) to reflect inherent quality. The ten previously degraded genomes begin with the lowest quality (highest entropy) and are barely affected by further degradation. This is the heart of our contention that “the higher the quality, the greater the vulnerability to degradation.”

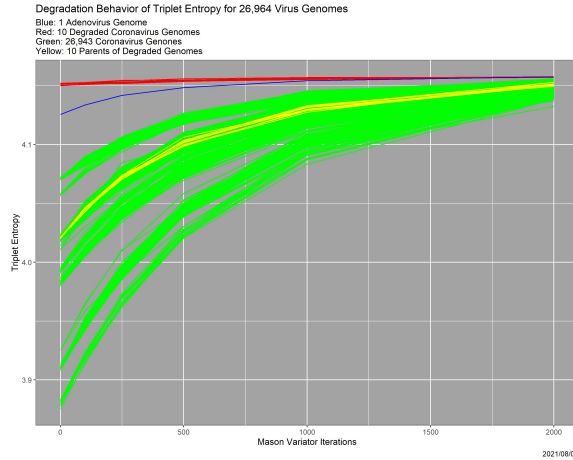


Figure 1: Effect of SNP degradation (Karr et al., 2022) on the entropy of 26964 virus genomes.

## 2.2 Scientific Context

As in Karr et al. (2022) and Karr et al. (2026), the scientific problem underlying this paper is to classify short (in our case, length 101) DNA sequences as having arisen from one of three candidate virus genomes. The broader context is reference-guided *metagenomic assembly*—piecing together fragments (reads) of DNA from multiple potential sources into longer sequences called contigs, as performed, for example, by MetaCompass (Cepeda et al., 2017; Pop, 2024), with the assistance of a (reference) database of sequenced candidate genomes. The role of the reference database is to reduce the computational burden of creating the contigs, which is formulated as finding an Eulerian path in a de Bruijn graph (Compeau et al., 2023). The medical setting involved samples from human digestive and reproductive tracts (Porter and Karr, 2024).

## 2.3 Classifiers

In this paper, a classifier is a function  $C$  from a finite input space  $\mathcal{I}$  to a finite output space  $\mathcal{O}$ . Elements of  $\mathcal{I}$  are *inputs* or *data*, and  $C(x) \in \mathcal{O}$  is the *decision* or *result* for input  $x$ . Although it is not a logical necessity, almost always  $|\mathcal{I}| \gg |\mathcal{O}|$ , where  $|\mathcal{S}|$  is the cardinality of the set  $\mathcal{S}$ .

Following Karr et al. (2026), we assume that the input space  $\mathcal{I}$  is an *loopless, undirected graph*, whose edgeset  $E$  defines neighboring inputs:  $x, y \in \mathcal{I}$  are *neighbors* if and only if  $x \neq y$  and  $\{x, y\} \in E$ . We denote by  $\mathcal{N}(x) = \{y : \{x, y\} \in E\}$  the set of neighbors, or neighborhood, of  $x$ . For ease of interpretation, we further assume that  $\mathcal{I}$  is *connected*: for any  $x, y \in \mathcal{I}$ , there is a path  $(x_1 = x, \dots, x_k = y)$  that connects them:  $\{x_j, x_{j+1}\} \in E$  for each  $j$ .

In this paper,  $\mathcal{I}$  consists of all Next Generation Sequencers (NGS)-generated DNA sequences of length 101. With five possible values for each nucleotide (see below for an explanation of the fifth value),  $|\mathcal{I}| = 5^{101}$ . With three candidate genomes,  $|\mathcal{O}| = 3$ . Neighboring reads differ in exactly one of 101 bases, which is known as a single nucleotide polymorphism (SNP).

## 2.4 Classifier Boundaries

The boundary  $\mathcal{B}$  associated with  $C$  is the set of elements of  $\mathcal{I}$  at least one of whose neighbors is classified differently:

$$\mathcal{B}_C = \{x \in \mathcal{I} : C(x') \neq C(x) \text{ for some } x' \in \mathcal{N}(x)\}. \quad (1)$$

For DNA reads, this means that there are points differing at only one base that are classified differently. Crucially, whenever two inputs are classified differently, any path in  $\mathcal{I}$  connecting them must contain at least two (neighboring) boundary points.

Below we focus on *Hamming paths*, which are the shortest. Given reads  $R \neq R'$  with Hamming distance  $k$  (They differ in  $k$  locations.), a Hamming path from  $R$  to  $R'$  replaces one differing nucleotide in  $R$  at a time by the corresponding nucleotide in  $R'$ . Therefore, each successive pair on the path are neighbors. Such a path ( $R_0 = R, \dots, R_k = R'$ ) has length  $k + 1$ ; there are  $k!$  of them. The “simplest” of these paths simply moves left to right in the character strings. Because  $C(R) \neq C(R')$ , there is at least one value of  $j$  for which  $C(R_j) \neq C(R_{j+1})$ , in which case, the neighbors  $R_j$  and  $R_{j+1}$  both belong to  $\mathcal{B}_C$ .

## 2.5 Surrogate Uncertainty Measures

The boundary engenders two measures of uncertainty that are applicable to any classifier whose input space is a graph Karr et al. (2026). For  $x \in \mathcal{I}$ , both are functions of the distribution on  $\mathcal{O}$  of  $\{C(x') : x' \in \mathcal{N}(x)\}$ . We define them in generality.

The *Boundary Status*, of  $x \in \mathcal{I}$  is the number of points in  $\mathcal{O}$  other than that assigned to  $x$  itself appearing among the decisions for its neighbors:

$$\text{BS}_C(x) = \sum_{z \in \mathcal{O}, z \neq C(x)} 1(z \in \{C(x') : x' \in \mathcal{N}(x)\}), \quad (2)$$

where  $1(\cdot)$  is an indicator function, equal to one if its argument is true and zero otherwise. In particular,  $\text{BS}_C(x) = 0$  means that all neighbors are classified the same as  $x$ , i.e.,  $x$  is not on the boundary. At the other extreme,  $\text{BS}_C(x) = |\mathcal{O}| - 1$  means that all of the other possible decisions appear among the neighbors. Note that  $\text{BS}_C(x)$  does not depend on whether  $C(x) \in \{C(x') : x' \in \mathcal{N}(x)\}$ .

The second measure, *Neighbor Similarity*, quantifies the extent to which the neighbors of a point have the same decision it does. The Neighbor Similarity for an input point  $x$  is

$$\text{NS}_C(x) = 1 - H(q_x, q_{\mathcal{N}(x)}), \quad (3)$$

where  $H$  denotes Hellinger distance (Nikulin, 2001),  $q_x$  is the degenerate probability distribution on  $\mathcal{O}$  concentrated on  $C(x)$ , and  $q_{\mathcal{N}(x)}$  is the probability distribution on  $\mathcal{O}$  of  $\{C(x') : x' \in \mathcal{N}(x)\}$ . Therefore,

$$\mathcal{B}_C = \{x \in \mathcal{I} : \text{NS}_C(x) < 1\}. \quad (4)$$

Unlike  $\text{BS}_C$ ,  $\text{NS}_C$  takes account only of *how many* neighbors differ, not their values.

Our principal proposed interpretation of  $\text{NS}_C(x)$  is as uncertainty regarding the classification of  $x$ . If  $\text{NS}_C(x) = 1$ , *all* neighbors of  $x$  have the same decision as  $R$ , and, intuitively, we would be more certain of the decision for  $x$ . At the other extreme, if  $\text{NS}_C(x)$  were zero, moving to any neighbor of  $x$  changes the decision, in which case we would be highly uncertain about  $C(x)$ . In the case study in Karr et al. (2026), this does not occur: the maximum number of differently classified neighbors is 393 (of 404).

However—and this is important, as discussed further in Section 4, we must distinguish certainty from correctness. In some regions of  $\mathcal{T}$ , Neighbor Similarity may be high because “everything” is assigned the same, but incorrect, value.

### 3 Experimental Protocol

Here we present the protocol for our numerical experiments,

#### 3.1 Mathematical Preliminaries

To establish notation, a DNA sequence  $S$  is a character string chosen from the nucleotide (base) alphabet  $\{A, C, G, T\}$ , where A is adenine, C is cytosine, G is guanine and T is thiamine. At one extreme,  $S$  may be an entire genome—for instance, a virus or a human chromosome. At another, it may be a read generated by a NGS. Given a sequence  $S$ , its length is  $|S|$ ; the  $i^{\text{th}}$  base in  $S$  is  $S(i)$ ; and the bases from location  $i$  to location  $j > i$  are  $S(i : j)$ .

We focus on triplets, whose distributions are 64-dimensional summaries of sequences. The *triplet distribution*  $P_3(\cdot|S)$  of a sequence  $S$  is defined as

$$P_3(b_1b_2b_3|S) = \text{Prob}\{S(k : k + 2) = b_1b_2b_3\} \quad (5)$$

for each choice of  $b_1b_2b_3$ , where  $b_1, b_2$  and  $b_3$  are elements of  $\{A, C, G, T\}$ , and  $k$  is chosen at random from  $1, \dots, |S| - 2$ . An equivalent perspective is that of a second-order Markov chain (Karr et al., 2023).

That triplets suffice in this setting is argued at length in Karr et al. (2026) and Karr et al. (2023). Briefly, the Hellinger distances between the triplet distributions for the three genomes are so large (Karr et al., 2026) that the triplet distributions differentiate the genomes. And, of course, triplets are fundamental biologically because they encode amino acids. Other cases appear in the literature, especially quartets, also referred to as tetranucleotides (Pride et al., 2003; Teeling et al., 2004a,b). In our experience, quartets are more burdensome computationally than triplets without being more useful.

#### 3.2 Training and Validation Datasets

As the “root” training dataset  $\mathcal{T}$  for all four classifiers (Section 3.3), we use the same dataset employed in Karr et al. (2022) and Karr et al. (2026). It consists of 5869 simulated NGS reads of length 101:

**Adeno:** 1966 reads from an adenovirus genome of length 34,125, downloaded with the read simulator `Art`;

**COVID:** 1996 reads from a SARS-CoV-2 genome of length 29,926 contained in a coronavirus dataset downloaded from National Center for Biotechnology Information (NCBI) in November, 2020;

**SARS:** 1907 reads from a SARS-CoV genome of length 29,751 from the same database as COVID.

Thus,  $\mathcal{O} = \{\text{Adeno}, \text{COVID}, \text{SARS}\}$ .

We employed the `Mason_simulator` software (Holtgrewe, 2010) to simulate Illumina NGS reads from each genome, with approximate 6X coverage. (Illumina manufactures NGSs that employ an optical technology; see <https://www.illumina.com/>.) `Mason_simulator` introduces errors in the form of transpositions (SNPs), insertions, deletions and undetermined bases. The latter are cases in which the

sequencer detects a nucleotide, but is unable to determine whether it is A, C, G or T. Following convention, these appear in the simulated reads as “N,” and must be accommodated in computations. Parameters of the `Mason_simulator` were set at default values.

The validation dataset  $\mathcal{V}$ , which we earlier also termed the analysis dataset, is effectively a clone of the training dataset, consisting of 2000 reads from each of the three genomes generated using the `Mason_simulator`. It is used to evaluate classifier performance.

### 3.3 The Four Classifiers

Here we introduce the four classifiers investigated in this paper, as well as compare their performance on the training dataset. Throughout, the response is the read source and the predictors are the triplet distribution for the read.

#### 3.3.1 Bayes Classifier

The first classifier is that in Karr et al. (2026). Three likelihood functions, denoted by  $L(\cdot|\text{Adeno})$ ,  $L(\cdot|\text{COVID})$ , and  $L(\cdot|\text{SARS})$ , are calculated from the triplet distributions. We assume a uniform prior  $\pi_R = (1/3, 1/3, 1/3)$  on  $\mathcal{O}$  for each read. We then use Bayes’ theorem and the three likelihoods to calculate posterior probabilities  $p(\cdot|R)$  over  $\mathcal{O}$ , which yield the classifier decisions  $C(R) = \arg \max_{x \in \mathcal{O}} p(x|R)$ . Table 1 contains the resultant confusion matrix for training dataset, which shows that the Bayes classifier performs well, albeit not spectacularly.

Table 1: Confusion matrix for the Bayes classifier and undegraded training data  $\mathcal{T}$ . The correct classification rate is 81.58%.

Source	Decision			Sum
	Adeno	COVID	SARS	
Adeno	1580	114	272	1966
COVID	58	1738	200	1996
SARS	253	184	1470	1907
Sum	1891	2036	1942	5869

#### 3.3.2 Neural Net Classifier

Our neural net is an “out-of-the box” version of the `neuralnet` package in R with default settings. The algorithm is resilient backpropagation with weight backtracking (Riedmiller, 1994), the activation function is logistic, and there is one hidden neuron per layer. The confusion matrix for  $\mathcal{T}$  is in Table 2.

#### 3.3.3 Partition Model Classifier

We employ a regression tree (Hastie et al., 2001), as implemented in the `rpart` package in R. Standard heuristics for pruning, which select a complexity parameter on the basis of 10-fold cross-validation, lead to

Table 2: Confusion matrix for the neural net classifier and undegraded training data  $\mathcal{T}$ . The correct classification rate is 76.20%.

	Adeno	COVID	SARS	Sum
Adeno	1626	40	300	1966
COVID	51	1724	221	1996
SARS	532	253	1122	1907
Sum	2209	2017	1643	5869

a tree with 549 terminal nodes, which is still clearly over-fitted. Instead, we pruned to a tree with 61 terminal nodes. The confusion matrix appears in Table 3.

Table 3: Confusion matrix for the partition model classifier and undegraded training data  $\mathcal{T}$ . The correct classification rate is 75.81%.

	0	1	2	
	Adeno	COVID	SARS	Sum
Adeno	1491	93	382	1966
COVID	130	1640	226	1996
SARS	333	256	1318	1907
Sum	1954	1989	1826	5869

### 3.3.4 Random Forest Classifier

This classifier is the R package `randomforest` with no modifications. Table 4 contains the confusion matrix.

Table 4: Confusion matrix for the random forest classifier and undegraded training data  $\mathcal{T}$ . The correct classification rate is 91.78%.

	0	1	2	Sum
Adeno	1815	62	89	1966
COVID	57	1896	43	1996
SARS	117	114	1676	1907
Sum	1989	2072	1808	5869

## 3.4 Structure of an Experiment

All of the experiments reported in Section 4 have the same structure, which we describe here.

**Training data:** Begin with training dataset  $\mathcal{T}$  from Section 3.2.

**Training data quality degradation:** Select a degradation method, which in most cases is parameterized in a way that represents increasing degradation, and apply it to the training dataset. For instance, in Section 4.1, we use the SNP probability-parameterized method employed in Karr et al. (2022).

**Classifier execution:** For each value of the degradation parameter, re-train all four classifiers on the degraded training dataset, and apply it to the (never altered) validation dataset  $\mathcal{V}$ .

**Classifier performance evaluation:** For each case (as defined above), summarize classifier behavior for the validation dataset  $\mathcal{V}$  in terms of

- Predictions, including the correct classification rate, and
- Boundary Status distribution.

In Section 4.1, these appear in Figures 3–5.

**Classifier congruence:** For each value of the degradation parameter, calculate the extent to which the classifiers concur, exemplified by Figure 6. As discussed below, one recurrent finding is that congruence often degenerates slowly as the data quality decreases, drops precipitously, then rises again.

## 4 Results and Findings

Before exploring details, we emphasize the clear message that *training data quality matters*.

For comparison with results below, Figure 2 contains the confusion matrices for  $\mathcal{V}$  for the four classifiers trained on the undegraded training dataset.

Source	Decision			Sum
	Adeno	COVID	SARS	
Adeno	1566	96	338	2000
COVID	58	1734	208	2000
SARS	253	232	1515	2000
Sum	1877	2062	2061	6000

Source	Decision			Sum
	Adeno	COVID	SARS	
Adeno	1649	42	309	2000
COVID	98	1741	200	2000
SARS	533	300	1167	2000
Sum	2241	2083	1676	6000

Source	Decision			Sum
	Adeno	COVID	SARS	
Adeno	1581	110	309	2000
COVID	117	1567	316	2000
SARS	399	281	1320	2000
Sum	2097	1958	1945	6000

Source	Decision			Sum
	Adeno	COVID	SARS	
Adeno	1744	65	191	2000
COVID	74	1831	95	2000
SARS	212	207	1581	2000
Sum	2020	2103	1867	6000

Figure 2: Confusion matrices for the validation dataset  $\mathcal{V}$  for the four classifiers trained on the undegraded training data  $\mathcal{T}$ . *Top left:* Bayes classifier. *Top right:* neural net. *Bottom left:* partition model. *Bottom right:* random forest

## 4.1 SNP Degradation

As mentioned previously, the degradation mechanism here is that of Karr et al. (2022). There is a parameter called `SNP_Probability` belonging to  $(0, 1)$ , and each base in a DNA sequence is changed to another value with that probability, independently of the others. The software used here and in Karr et al. (2022) is the `Mason_variator` (Holtgrewe, 2010). The mechanism mimics nature because the changes are SNPs.

In most cases, the values of `SNP_Probability` are

$$\{0, 0.01, 0.05, 0.10, 0.25, 0.50, 0.60, 0.65, 0.70, 0.75, 0.80, 0.85, 0.90, 0.95\},$$

and the randomization is done independently at each step, as opposed to successively degrading additional reads.

The results appear in Figures 3–6. They are at once unsurprising and unexpected. Starting with Figure 3, that correctness decreases as `SNP_Probability` increases is completely expected. Until `SNP_Probability` is approximately 0.75, the decrease is linear, and the rate of decrease is essentially the same for all four classifiers. What happens in the vicinity of `SNP_Probability` = 0.75 is, to least to us, unforeseen. Performance of all four classifiers drops precipitously, and never recovers. This breakdown behavior appears in other cases below, again uniformly across the four classifiers, so it seems not to be a function of the classifier or the mode of degradation.

Figure 4 begins to illuminate the situation. Starting at the breakdown, almost all predictions become Adeno, again for all four classifiers. That is, once the training data are degraded sufficiently, the classifiers lose predictive power. This also explains why the number of correctly classified reads does not become zero in Figure 3, because those from the Adeno genome are classified correctly. It is not clear why Adeno, rather than COVID or SARS, becomes the default prediction for classifiers trained on what is effectively noise.

In Figure 5, things become more complex, and the four classifiers no longer behave identically. The behaviors for the Bayes classifier, the neural net and the random forest are qualitatively similar. The Boundary Status distribution is relatively stable when `SNP_Probability` < 0.75, with a slight increase in the proportion of validation dataset reads with `BS` = 0, then there is a sharp drop in the number of validation dataset reads with `BS` = 0 (with most of the compensating increase being `BS` = 1). Past `SNP_Probability` = 0.75, the increase in the proportion with `BS` = 0 resumes. Among these three, the random forest stands out because of the sharp increase in `BS` = 2, and corresponding decrease in `BS` = 0. The behavior in these three cases is consistent with the preceding paragraph. For `SNP_Probability` < 0.75, the boundary composition is relatively constant. At `SNP_Probability` = 0.75, it changes dramatically, with `BS` values of 1 and 2 becoming much more prevalent. Once `SNP_Probability` > 0.75, as everything is predicted to be Adeno, the boundary starts to disappear. Not that the boundary is ever small. The fraction of validation dataset reads for which `BS` = 0 is essentially never above .8 until the classifiers degenerate into predicting everything to be Adeno.

The partition model differs from the other three classifiers in that its boundary is much larger. The proportion of validation dataset reads with `BS` = 0 is the smallest of the three, and never exceeds 0.3. This means that of 70% validation dataset reads lie on the boundary. But still something happens in the vicinity of `SNP_Probability` = 0.75, followed by a return to the behavior for `SNP_Probability` < 0.75. The partition model is also an outlier in other cases below.

Figure 6 completes the story. It shows that six pairwise congruences between the classifiers—the numbers of reads for which they agree, as well as the four-way congruence. The differences among the pairwise congruences are meaningful, and we return to them momentarily. The overall message reinforces the preceding discussion. For `SNP_Probability` < 0.75, congruences are high, and because all four of the classifiers

are generally correct. Around  $\text{SNP\_Probability} = 0.75$ , the congruences go haywire. For  $\text{SNP\_Probability} > 0.75$ , they become high again, but because the four classifiers are incorrect in the same way: each classifier is predicting “all Adeno.” There results an interesting implication regarding ensemble methods. For  $\text{SNP\_Probability} < 0.75$  (higher quality training data), ensembling may not help because the four classifiers may generally be correct, whereas for  $\text{SNP\_Probability} > 0.75$  (lower quality training data), it may not help because all have degenerated in the same way.

The pairwise congruences in Figure 6, while qualitatively similar, are not identical quantitatively. Moreover, they are ordered numerically in a way that is largely independent of  $\text{SNP\_Probability}$ . That for Bayes–random forest is highest, followed by Bayes–neural net, then neural net–random forest, then partition model–random forest, Bayes–partition model, and neural net–partition model. Although we do not pursue the issue here, the partition model seems to be the most deviant.

For this case only, results for Neighbor Similarity appear in Figures 32–35, which we have placed in Appendix A because of their size. There is one figure for each classifier, and within each, one panel per value of  $\text{SNP\_Probability}$ . The graphs are of densities of the associated values of Neighbor Similarity. Blank panels correspond to cases where Neighbor Similarity is identically one, so that there is no density function. Figure 32, for the Bayes classifier, is consistent with other interpretations. For low and high values of  $\text{SNP\_Probability}$ , Neighbor Similarity is high, for different reasons. In the vicinity, of  $\text{SNP\_Probability}$ , it deteriorates. Behavior for the neural net (Figure 33) is similar, with less pronounced deterioration. By contrast, for the random forest (Figure 35), the deterioration becomes true breakdown. The partition model (Figure 34) is truly different. We simply cannot explain, or even hypothesize a reason for, the persistent trimodality in the distribution of Neighbor Similarity. The deterioration as  $\text{SNP\_Probability}$  increases, which appears as a leftward shift in the modes, remains.

Finally, an interesting complementarity for the Bayes classifier appears in Karr et al. (2026), but there with respect to the quality of the validation dataset with the training dataset held constant and undegraded. If  $\mathcal{V}$  is replaced by random reads, or reads from bacterial or human genomes, the more distant those are from the training data, the more the decisions for it degenerate into “all Adeno.”

The big question, of course, is “Why  $\text{SNP\_Probability} = 0.75$ ?” We defer this to Section 5.

## 4.2 Variants of SNP Degradation

Here we discuss several variants of the degradation in Section 4.1. Before doing so, we note that the experiment in that section was replicated in its entirety, with results that were virtually identical. For brevity, we include the resultant analog of Figure 6, namely Figure 7. The two are virtually identical.

Nor is anything about the preceding results associated with the read length. Changing the read length to 200 makes no difference. The three panels in Figure 8 are virtually identical to the corresponding panels in Figure 4, even the to shapes of the plotted lines. Breakdown occurs at  $\text{SNP\_Probability} = 0.75$ . Figure 9, however, presents complications. While the breakdown is evident, and reproduces Figure 6, the early decline in all congruences involving the random field classifier is novel. There is recovery as  $\text{SNP\_Probability}$  approaches 0.5, but we lack an explanation. It simply be random variation, because none of our experiments other than the first one has yet been replicated, and even for that one, there are only two replicates.

To control the length of the paper, for the other variants in this section, we include only the figures for predictions and classifier congruence. Also, because of the computational burden associated with the Bayes classifier and since it is treated in detail in Karr et al. (2026), we have omitted it.

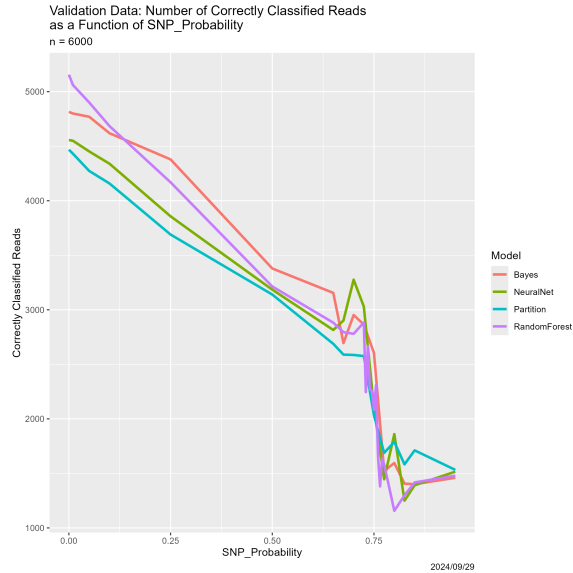


Figure 3: SNP degradation: number of correctly classified elements of  $\mathcal{V}$  as a function of SNP\_Probability.

#### 4.2.1 Initially Degraded Training Data

Especially in light of Figure 1, it is natural to wonder what happens if the initial training data are degraded. Especially, does the breakdown move to the left, meaning that it depends on the absolute degradation? Or, does it remain at 0.75, meaning that degradation is relative?

We ran two experiments. In the first, the initial training data are the original training dataset  $\mathcal{T}$  degraded with SNP\_Probability = 0.9. In the second, the initial training data are the original training data  $\mathcal{T}$  degraded with SNP\_Probability = 0.5. Predictions from them are in Figure 10 and congruence for the neural net, partition model and random forest in Figure 11.

Figure 10 should be compared to Figure 4, ignoring the Bayes classifier results in the upper left-hand panel of the latter. Qualitatively, they are very similar. Unambiguously, the breakdown is still present, and remains at SNP\_Probability = 0.75. The same is true in Figure 11, whose parallel is Figure 6. That is, the answer to the question in the first paragraph of this section is definitively that breakdown is relative. This is, we believe, as it should be. Whatever the training data are, the classifiers treat it as truth. If truth is wrong, they are wrong. Classifiers cannot be aware of any unobserved “prior truth.”

#### 4.2.2 Selective SNP Degradation

This experiment can be viewed as addressing the interpretations put forth in Section 4.1. If a random set of reads in  $\mathcal{T}$  are selected for degradation, say with probability Sel\_Probability, and each is degraded with probability SNP\_Probability, what happens? This scenario differs from that in Section 4.1 in sense that there, once SNP\_Probability is even moderately large, all reads are altered, whereas here, the degradation is confined to a subset of reads.

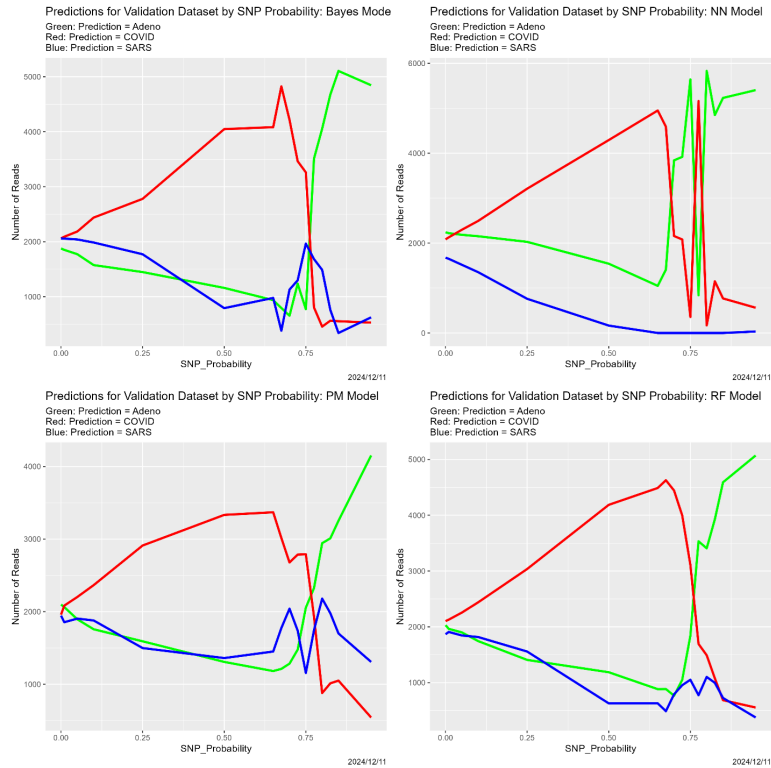


Figure 4: SNP degradation: classifier predictions as a function of SNP\_Probability. *Upper left*: Bayes classifier. *Upper right*: neural net. *Lower left*: partition model. *Lower right*: random forest.

So there are now two parameters, Sel\_Probability and SNP\_Probability, both ranging over

$$\{0.05, 0.15, 0.25, 0.35, 0.45, 0.55, 0.65, 0.70, 0.75, 0.80, 0.85, 0.95\}$$

in a full factorial design. For brevity, we consider only the three-way congruence among the neural net, partition model and random forest. Figure 12 contains both a heatmap and a 3-dimensional surface showing it. The most striking feature is that breakdown persists, but only when both probabilities reach 0.75. There is degeneration when one is small and the other large (the upper left-hand and lower right-hand corners in the heatmap), but it is relatively minor. There is also asymmetry between Sel\_Probability and SNP\_Probability, but it is subtle and requires further investigation before we assert its existence with confidence. We find only limited evidence of a return to congruence following breakdown, but we suspect that this is due to our not including probabilities greater than 0.95.

Can congruence be modeled as a function of Sel\_Probability and SNP\_Probability? The minor asymmetry notwithstanding, by a symmetric function, from Figure 12, a plausible candidate is the minimum of the two, and indeed the adjusted  $R^2$  for the model is 0.8256. However, which is crucial, the model dramatically overpredicts congruence once the minimum exceeds 0.75. Put differently, it cannot predict the post-breakdown decline in congruence.

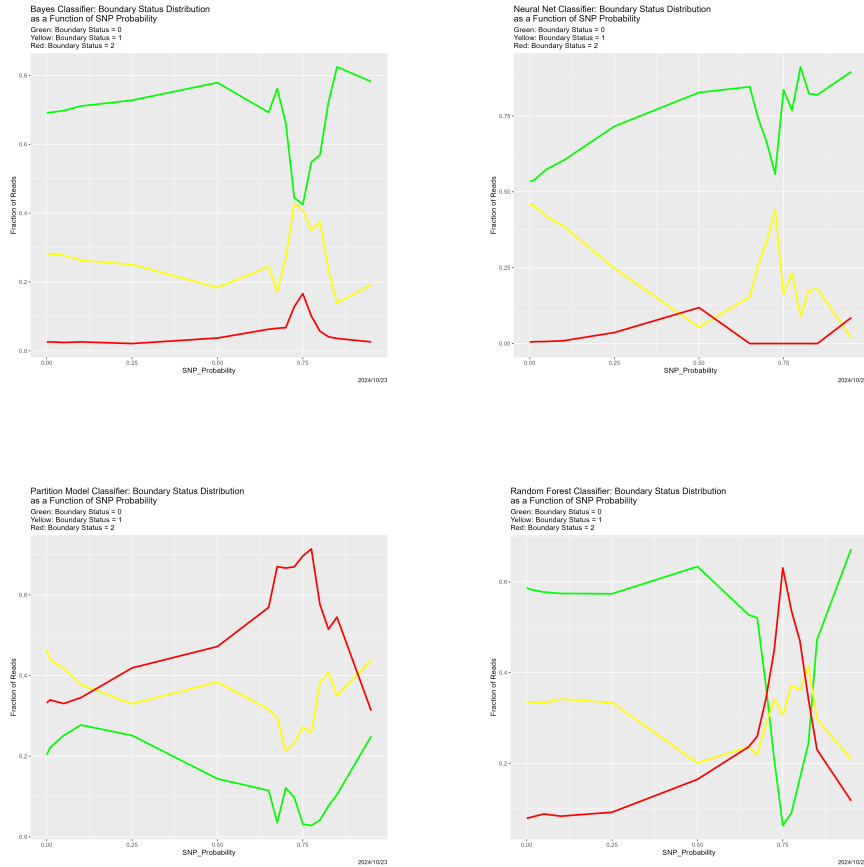


Figure 5: SNP degradation: Boundary Status distribution as function of SNP\_Probability. *Upper left:* Bayes classifier. *Upper right:* neural net. *Lower left:* Partition model. *Lower right:* random forest. In each of these, BS = 0 is the green line, BS = 1 is the yellow line, and BS = 2 is the red line.

### 4.2.3 Protecting Some Read Sources

Here we explore the effect of exempting reads from particular sources from degradation. One motivation is to accommodate laboratory effects, in the sense that the quality of gene sequence data may depend on the laboratory that generated them, a phenomenon that is demonstrably present in Karr et al. (2023).

Such protection can be done in six ways, of course: protect reads whose source is one genome, or protect all reads except those whose source is one genome. The central question is whether the effects, especially prediction, are localized in the same way. Nor is “full protection” necessary: the experiment in Section 4.1 could instead have three SNP\_Probabilities, one for each genome. This is a direction we begin to explore in Section 4.3.5.

Figures 13–15 show predictions from the “protect one genome” scenario, with congruence in Figure 16. Here the story differs from previous (and subsequent) experiments. In none of Figures 13–15 is there more than mild evidence of breakdown, although what evidence there is, for example in Figure 15, continues to point to SNP\_Probability = 0.75 as the location. The stronger message is that as reads from two of the

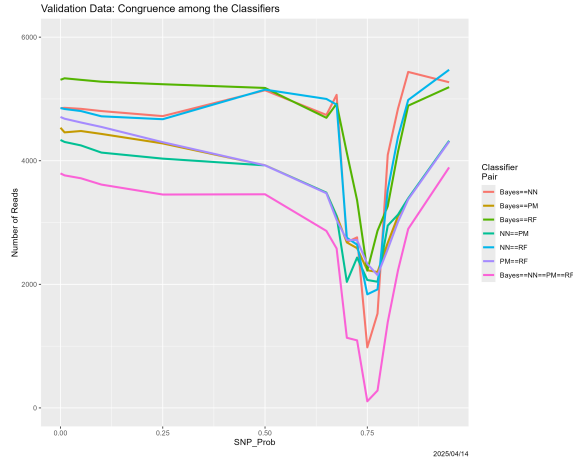


Figure 6: SNP degradation: classifier congruence as a function of SNP\_Probability.

genomes are degraded, predictions all become the undegraded genome. This is true for all three genomes and all three classifiers. This is sobering: when there is *differential data quality* in  $\mathcal{T}$ , predictions may be incorrectly “forced” onto higher quality results because the real validation data look more like high quality training data than like noise.

Figures 17–19 show predictions from the “degrade only one genome” scenario. Congruence is in Figure 20. The results reinforce those for “protecting one genome.” Uniformly across genomes and classifiers, predictions are increasingly diverted from the one affected genome to the two genomes. Evidence of breakdown is, interestingly, different and not uniform. In Figure 18, something is happening in the vicinity of SNP\_Probability = 0.25 for all three classifiers. There is no hint of this in Figures 17 and 19. Whether something is happening in Figure 19 for values of SNP\_Probability in the vicinity of 0.8 is even less clear, because in any event, it is not happening for random forests. But, then is something happening for random forests at SNP\_Probability = 0.60?

### 4.3 Other Quality Problems

Here we address the question of whether the behavior described in Section 4.1 is specific to SNP-degradation, or holds as well for ways of decreasing data quality.

#### 4.3.1 Mislabeled Reads

All four of the classifiers depend on labeled training data. What happens if there are problems with the labeling process, as there inevitably are in reality? In the experiment described next, randomly selected elements of  $\mathcal{T}$  have their labels changed. The Mislabeled\_Probability varies over

$$\{0, 0.05, 0.15, 0.25, 0.35, 0.45, 0.55, 0.65, 0.70, 0.75, 0.80, 0.85, 0.95\}.$$

The results, in Figures 21 and 22, are ambiguous compared to those in previous sections. Starting with the former, predictions by the partition model are largely insensitive to Mislabeled\_Probability. Those for the

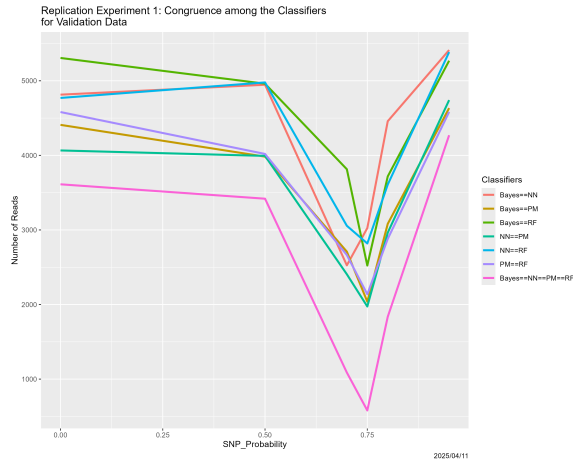


Figure 7: SNP degradation: classifier congruence as a function of SNP\_Probability for the *replicated version* of the experiment from Section 4.1.

random forest begin to diverge when Mislabeled\_Probability reaches approximately 0.75 (again!). The neural net seems inexplicably erratic. The disappearance of SARS from its predictions mirrors random forests, but is much more extreme and begins for much smaller values of Mislabeled\_Probability. The two extreme oscillations between predictions of Adeno and predictions of COVID have no analogues elsewhere in our experiments.

And yet, Figure 22 echoes its predecessors, although the minimum values congruence appear to be for Mislabeled\_Probability less than 0.75.

### 4.3.2 Reversed Reads

This is one case where we correctly expected nothing to happen. Recalling that DNA molecules are double helices (Watson, 2001), there is inherent uncertainty in NGS reads regarding which strand they come from. (Sequenced genomes have a well-determined 5' end, characterized by a free phosphate, and 3' end, characterized by a free hydroxyl.) Therefore, reversing some reads, as character strings, should have minimal effect. Figures 23 and 24 confirm this expectation.

### 4.3.3 Reduced Training Data

Here we explore the effect of a more global quality characteristic of training data—their size and balance. Recall from Section 3.2 that  $\mathcal{T}$  contains approximately equal numbers of Adeno, COVID and SARS reads, so does  $\mathcal{V}$ , both of which may matter. In each run of this experiment, reads with a specified source are deleted at random from  $\mathcal{T}$ , so that the experiment is parameterized by a Removal\_Probability taking values in

$$\{0, 0.05, 0.15, 0.25, 0.35, 0.45, 0.55, 0.65, 0.70, 0.75, 0.80, 0.85, 0.95\}.$$

There is no reason to expect that, if there is breakdown-like behavior, it will occur at Removal\_Probability = 0.75. There is, of course, reason to suspect that as reads from one source are removed, the number of

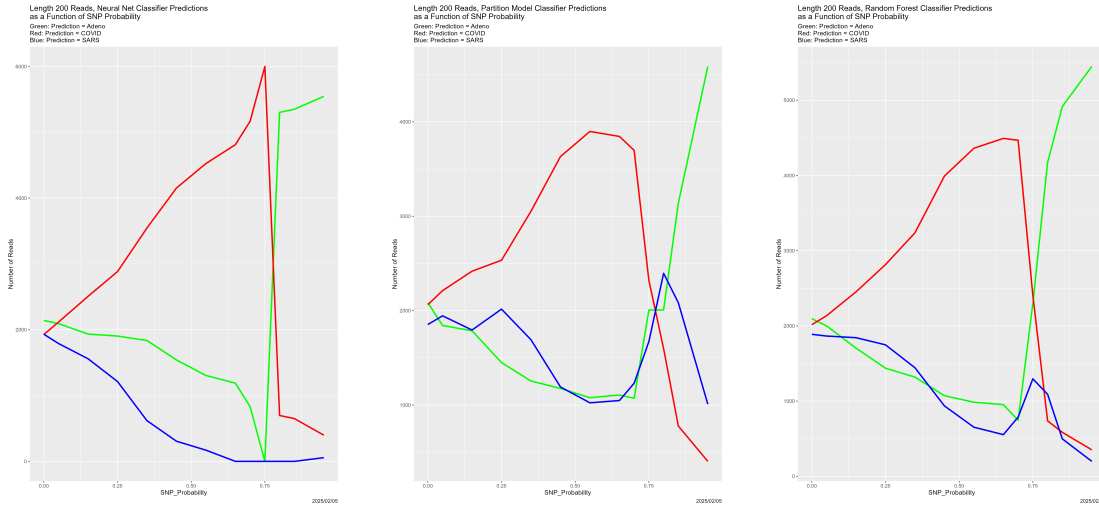


Figure 8: Length 200 reads: classifier predictions as a function of SNP\_Probability. *Green*: prediction = Adeno. *Red*: prediction = COVID. *Blue*: prediction = SARS.

elements in  $\mathcal{V}$  predicted to be from that source will decrease.

Prediction results appear in Figures 25–27, and congruence in Figure 28. Regarding predictions, the disappearance of prediction associated with removed reads happens smoothly and uniformly across removal source and classifiers. For the neural net, it disappears entirely for all three genomes in the vicinity of Removal\_Probability = 0.70. We have no explanation for the oscillation of the neural net with removed Adeno reads at Removal\_Probability = 0.75. which is also reflected in the congruences that involve the neural net. We find no other evidence of breakdown.

#### 4.3.4 Superfluous Training Data

It may seem paradoxical that too much data can be a data quality problem, especially if they are of high quality, but here we demonstrate that this is so. Moreover, our proposed explanation gibes perfectly with the overall themes of the paper. Intuitively and surely over-simplistically, a classifier that is trained to recognize data not in  $\mathcal{V}$  is wasting its finite potential.

The experiment is as follows: we create a superfluous dataset  $\mathcal{S}$  containing 12,000 *E. coli* reads, 785 reads from the Avian flu virus H5N1, 475 reads from Human Papillomavirus (HPV), 453 reads from Norovirus, and 477,357 reads from *P. Gingivalis*, a bacterium associated with chronic periodontitis. Its total size is 491,070. The “laundry list” feel reflects the varying sizes of the genomes with which we have worked. None of these is a close relative of the three virus genomes in  $\mathcal{T}$ . The validation data  $\mathcal{V}$  remain unchanged. As suggested above and confirmed below, training a classifier to recognize reads present are not in  $\mathcal{V}$  is actually counterproductive, and not simply wasteful. The experiment is parameterized by an Add\_Probability taking values in

$$\{0, 0.001, 0.005, 0.01, 0.05, 0.1, 0.2, 0.3, 0.4, 0.5, 0.6, 0.7, 0.8, 0.9, 1\},$$

which is applied each element of  $\mathcal{S}$  is added to  $\mathcal{T}$  before re-training the classifiers. The classifiers are applied to the unaltered validation data.

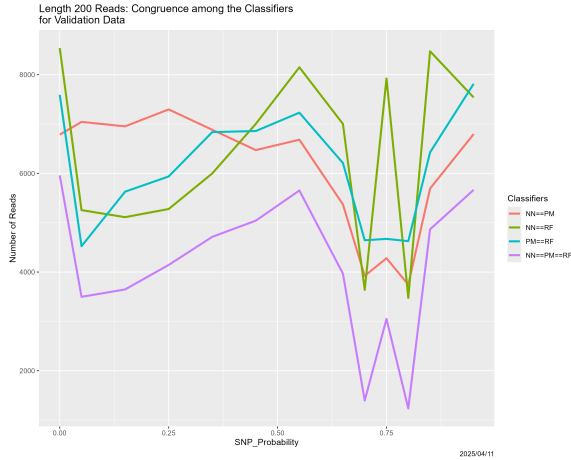


Figure 9: Length 200 reads: classifier congruence as a function of SNP\_Probability.

The usual results appear in Figures 29–31. There is mixed evidence, at best, of breakdown, but seemingly evidence of another form of instability entirely. Once there is any additional of superfluous reads (for Add\_Probability = 0.001, an average of 491 elements of  $\mathcal{S}$  are added to  $\mathcal{T}$ , which seems relatively innocuous), Adeno and SARS vanish from the predictions for the neural net. They vanish almost as rapidly for the random forest, and more slowly for the partition model. For these latter two, COVID also ultimately disappears from the predictions, but more slowly. It does not disappear for the neural net. This may be another instance of being right for the wrong reason.

Figure 29 shows, quite expectedly, that as more and more superfluous reads are added to  $\mathcal{T}$ , the overwhelming majority of which are *P. Gingivalis*, they overwhelm the predictions for  $\mathcal{V}$ . However, even for relatively small values of Add\_Probability, predictions are “siphoned off.” For instance, for the partition model, which seems to be the most vulnerable of the three, even at Add\_Probability = 0.001, 107 (of 6000) predictions are shifted to *P. Gingivalis*.

The Boundary Status distributions in Figure 30 are equally intriguing. For all three classifiers, once there are superfluous reads, the boundary virtually disappears—and rapidly. Combined with the prediction results, we see a false sense of security from the superfluous data, at least if Neighbor Similarity were used as a confidence measure.

Regarding congruence, there is a breakdown for Add\_Probability = 0.01, but with no recovery for the neural net. The partition model–random forest congruence, the breakdown is mild, and recovery occurs.

Clearly there is much more to be learned about this case, but the message to “be very afraid” of using a classifier when  $\mathcal{T}$  and  $\mathcal{V}$  are far apart is unmistakable. It is, of course, not a new message, but our work provides a more nuanced understanding of it.

#### 4.3.5 Mixed Data Quality Problems

Finally, as we have intimated previously, there is no reason to consider only one form of data quality degradation per experiment. Indeed the spirit of total survey error demands so. Here, we mix the SNP degradation of Section 4.1 with the mislabeling of Section 4.3.1. There are, then, three parameters:

- Sel\_Probability, the probability that each read in  $\mathcal{T}$  is selected for degradation;
- SNP\_Fraction, the conditional probability that a read selected for degradation is subject to SNP degradation—otherwise it is subjected to mislabeling;
- SNP\_Probability, with the same meaning as previously: given that a read is selected for SNP degradation, the probability with which each nucleotide in it is changed.

Potential values are

$$\{0.05, 0.15, 0.25, 0.35, 0.45, 0.55, 0.65, 0.70, 0.75, 0.80, 0.85, 0.95\}$$

for Sel\_Probability and SNP\_Probability, and

$$\{0.05, 0.15, 0.25, 0.35, 0.45, 0.55, 0.65, 0.75, 0.85, 0.95\}$$

for SNP\_Fraction.

And we introduce one further consideration, which whether we can model the contributions of the parameters to congruence. *A priori*, based on results above, congruence should decrease as either Sel\_Probability or SNP\_Probability increases. Whether it increases with SNP\_Fraction sheds light on which of the two forms of degradation is more injurious. A full factorial design of 1440 cases was not feasible computationally, so we instead used a 25-point Fedorov design explicitly meant to support fitting linear models (Fedorov, 1972; Wheeler, 2004). It and the associated results appear in Table 5.

We then fitted linear models with each of the four congruences as the response and the three parameters of the experiment as predictors. This is not a modeling decision informed by science, but is a reasonable place to begin. Addition of quadratic terms, as might be proposed based on the modeling discussion in Section 4.2.2, does not improve model fit. The four models are consistent with one another, and with the exception of that for NN\_RF, all fit the data comparably. The intercepts, which are the congruences in the absence of degradation, are consistent with those in previous sections. For all four models, the coefficient of Sel\_Probability is strongly negative and highly significant: the more overall degradation, the lower the congruence. While in no case is the coefficient of SNP\_Probability significant, it is always negative: more SNPs mean less congruence. And finally, the coefficient of SNP\_Fraction, while again not significant, is always positive and of the same order to magnitude. The interpretation is that shifting from Mislabeling to SNP degradation *increases* congruence, meaning that the former is more disruptive.

Table 5: Mixed degradation: experimental design and congruence among neural net, partition model and random forest.

Sel_Prob	SNP_Frac	SNP_Prob	NN_PM	NN_RF	PM_RF	NN_PM_RF
0.050	0.050	0.050	4165	4809	4549	3822
0.150	0.050	0.050	4191	4695	4541	3770
0.850	0.050	0.050	2334	2770	2410	1135
0.950	0.050	0.050	2722	3171	2777	1555
0.950	0.150	0.050	2582	3734	2569	1704
0.050	0.850	0.050	4229	4872	4623	3917
0.950	0.850	0.050	3910	4652	4441	3561
0.050	0.950	0.050	4363	4882	4728	4032
0.850	0.950	0.050	4028	4833	4485	3735
0.950	0.950	0.050	4257	4792	4602	3886
0.050	0.050	0.150	4202	4849	4578	3866
0.050	0.950	0.150	4243	4826	4653	3912
0.950	0.050	0.850	2956	3970	2821	2031
0.050	0.950	0.850	4228	4778	4679	3893
0.950	0.950	0.850	2247	3017	2400	1188
0.050	0.050	0.950	4268	4787	4704	3938
0.150	0.050	0.950	3982	4730	4394	3644
0.850	0.050	0.950	2626	3409	2714	1602
0.950	0.050	0.950	3076	3841	3167	2179
0.050	0.150	0.950	4240	4866	4625	3923
0.050	0.850	0.950	4166	4835	4642	3874
0.950	0.850	0.950	3299	4716	3072	2711
0.050	0.950	0.950	4175	4809	4591	3860
0.850	0.950	0.950	2535	2835	3082	1632
0.950	0.950	0.950	2569	3632	2825	1746

Table 6: Estimated coefficients and adjusted  $R^2$ -values for linear models of congruence as a function of Sel\_Pobability, SNP\_Fraction and SNP\_Probability. Labels for statistical significance are the standard ones.

Response	Predictors				Adjusted $R^2$
	Intercept	Sel_Prob	SNP_Frac	SNP_Prob	
NN_PM	4305.3 (***)	-1383.1 (***)	336.6	-365.6	0.6403
NN_RF	4818.8 (***)	-1157.4 (***)	344.1	-232.8	0.4468
PM_RF	4670.7 (***)	-1669.5 (***)	515.6	-418.9	0.6794
NN_PM_RF	3964.7 (***)	-1934.0 (***)	576.3 (.)	-462.3	0.6374

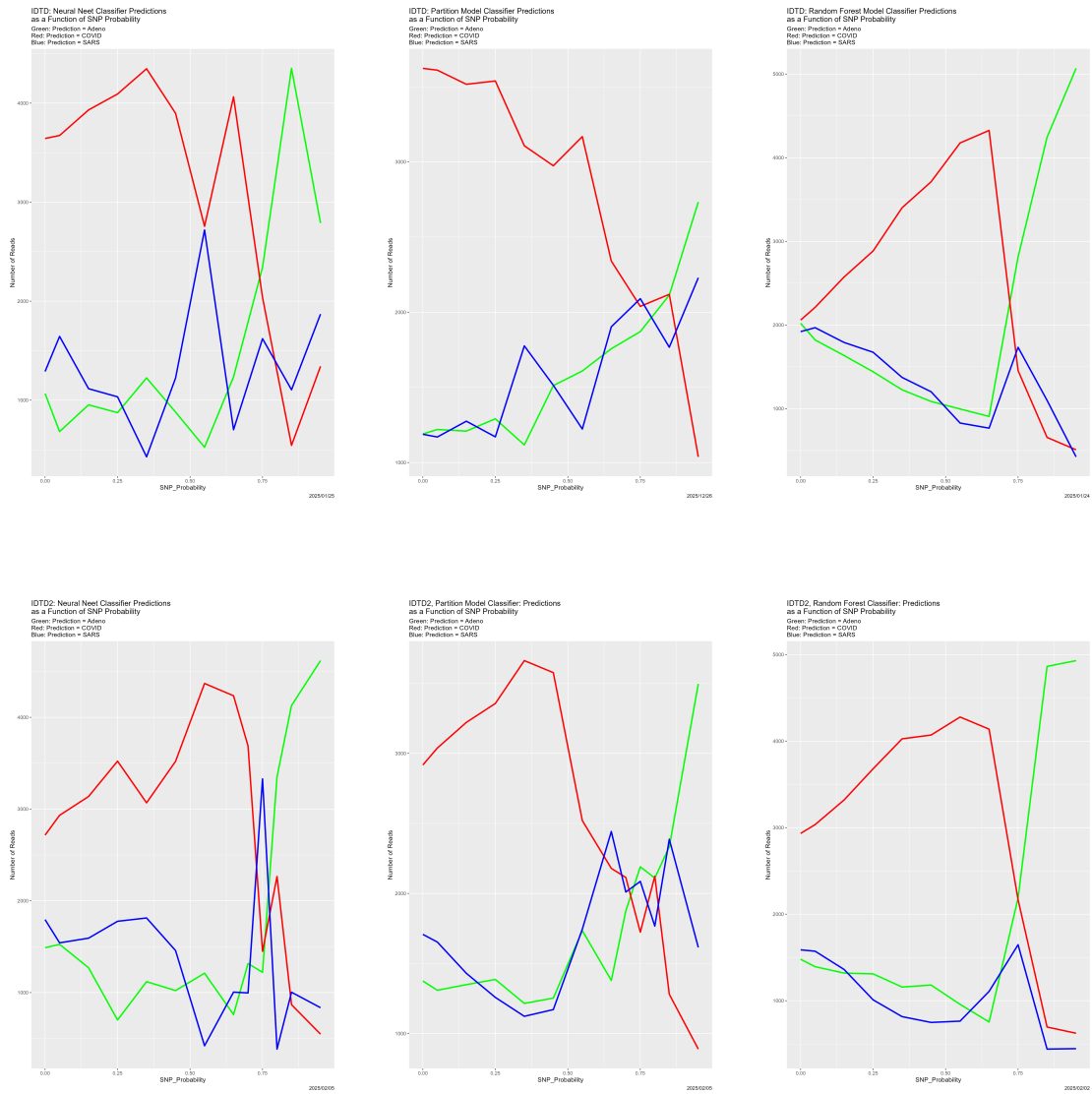


Figure 10: Initially degraded training data: classifier predictions as a function of SNP\_Probability. *Top:* SNP\_Probability for initial degradation is 0.9. *Bottom:* SNP\_Probability for initial degradation is 0.5. *Green:* prediction = Adeno. *Red:* prediction = COVID. *Blue:* prediction = SARS.

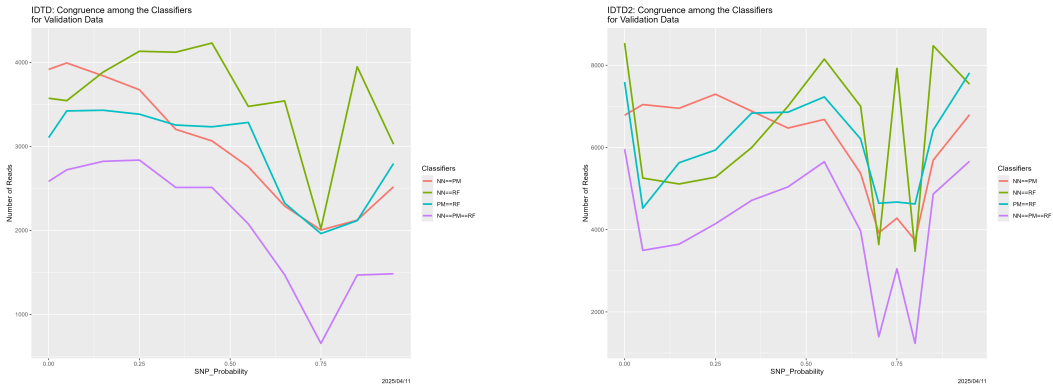


Figure 11: Initially degraded training data: classifier congruence as a function of SNP\_Probability. *Left:* SNP\_Probability for initial degradation is 0.9. *Right:* SNP\_Probability for initial degradation is 0.5.

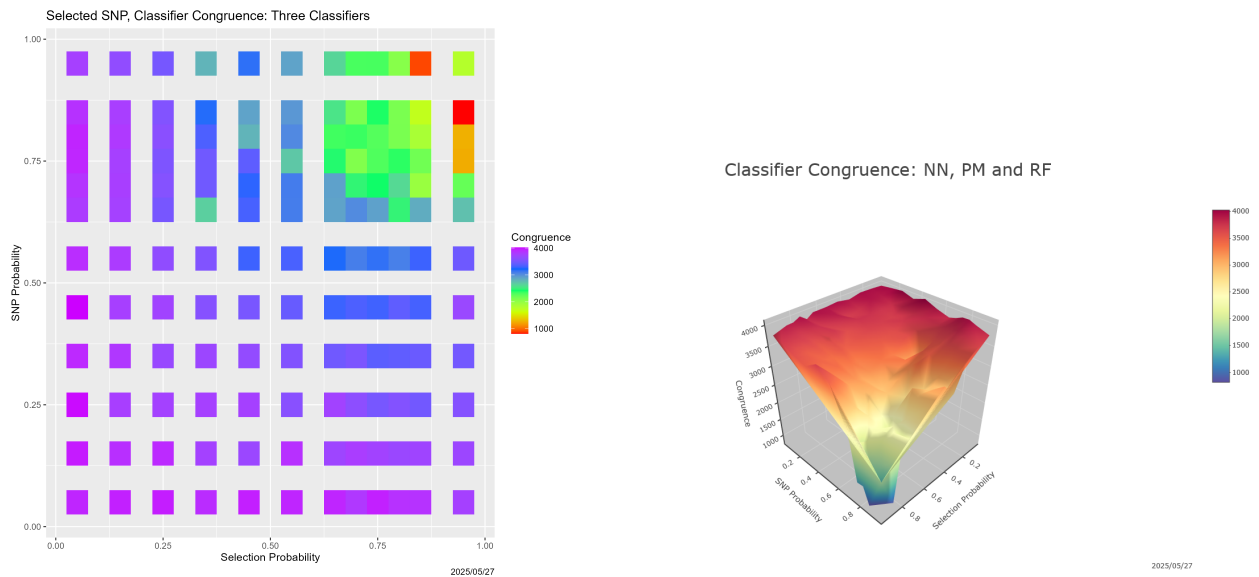


Figure 12: Selective SNP degradation: 3-way classifier congruence as a function of Sel\_Probability and SNP\_Probability. *Left:* heatmap. *Right:* 3D surface.

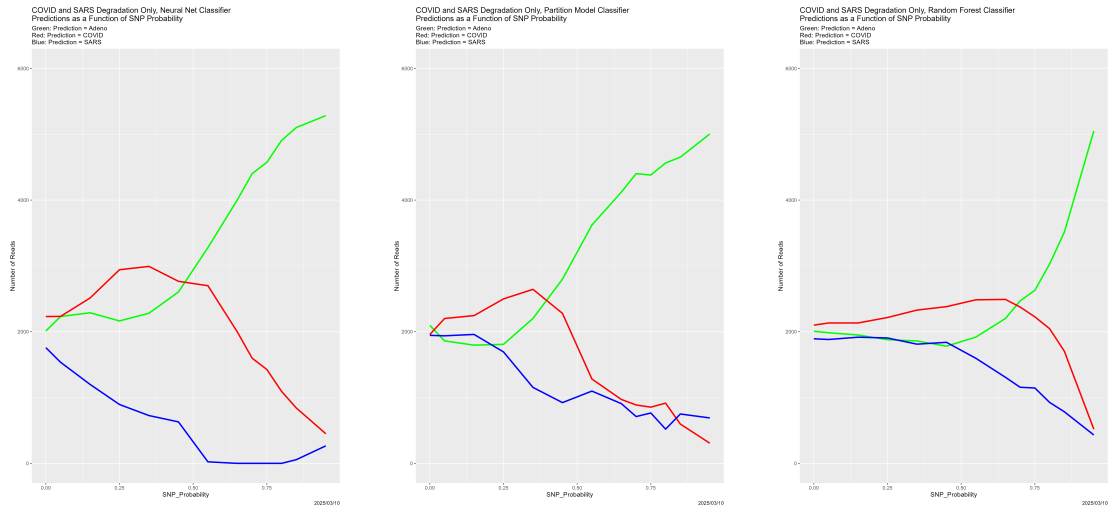


Figure 13: SNP degradation not applied to Adeno reads: classifier predictions as a function of SNP\_Probability. *Left*: neural net. *Center*: partition model. *Right*: random forest. *Green*: prediction = Adeno. *Red*: prediction = COVID. *Blue*: prediction = SARS.

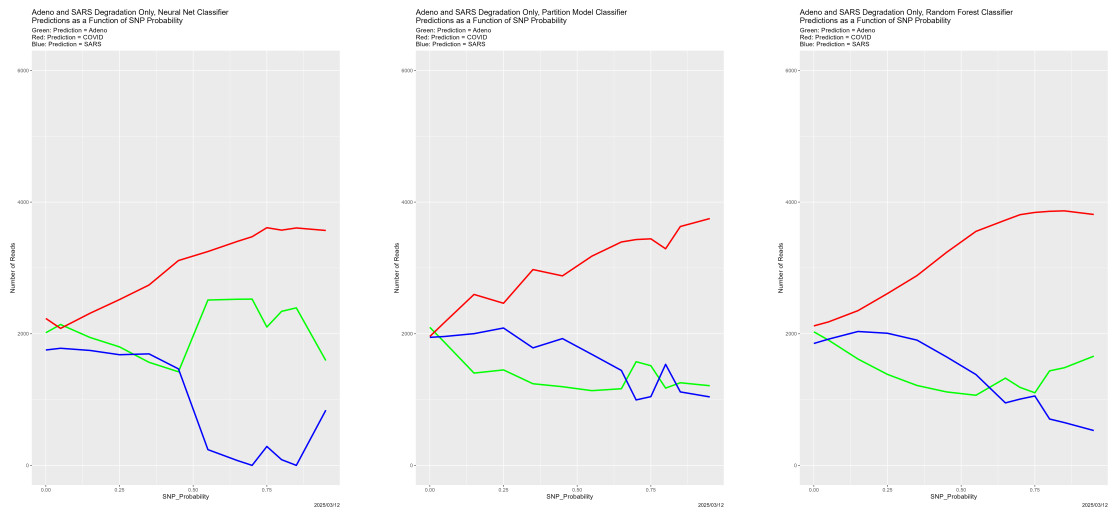


Figure 14: SNP degradation not applied to COVID reads: classifier predictions as a function of SNP\_Probability. *Left*: neural net. *Center*: partition model. *Right*: random forest. *Green*: prediction = Adeno. *Red*: prediction = COVID. *Blue*: prediction = SARS.

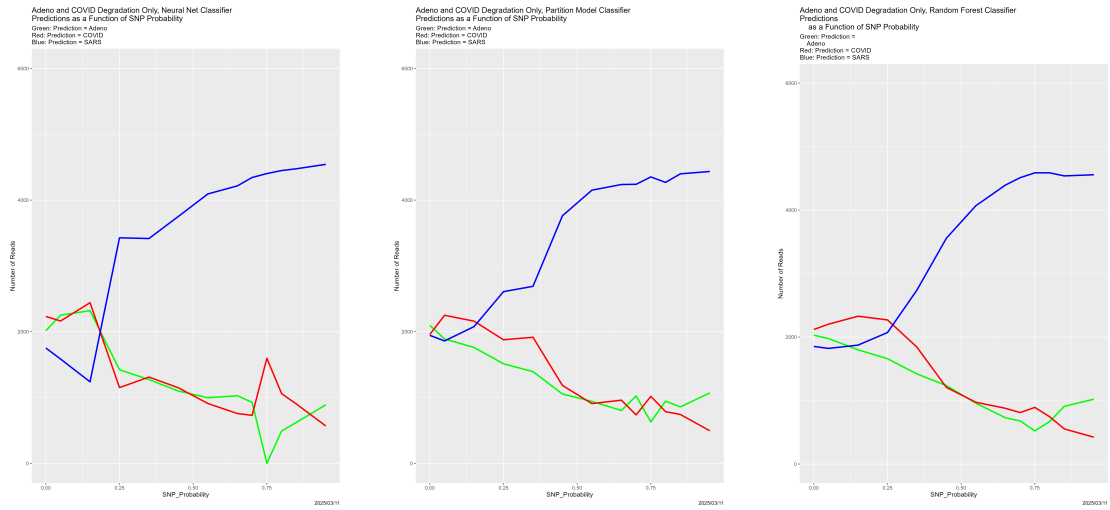


Figure 15: SNP degradation not applied to SARS reads: classifier predictions as a function of SNP\_Probability. *Left*: neural net. *Center*: partition model. *Right*: random forest. *Green*: prediction = Adeno. *Red*: prediction = COVID. *Blue*: prediction = SARS.

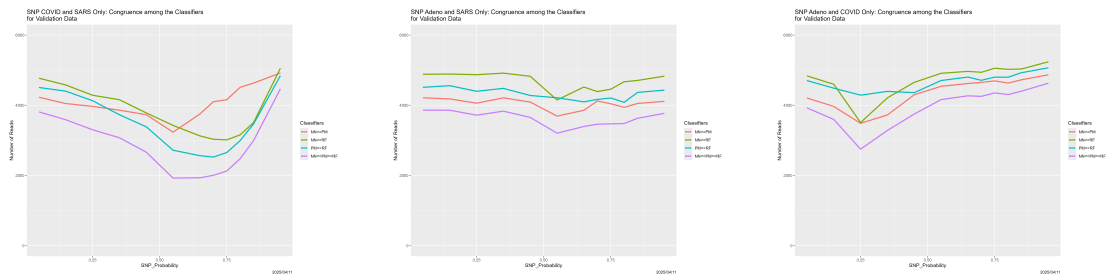


Figure 16: SNP degradation not applied to one set of reads: classifier congruence as a function of SNP\_Probability. *Left*: not applied to Adeno reads in training data. *Center*: not applied to COVID reads in training data. *Right*: not applied to SARS reads in training data.

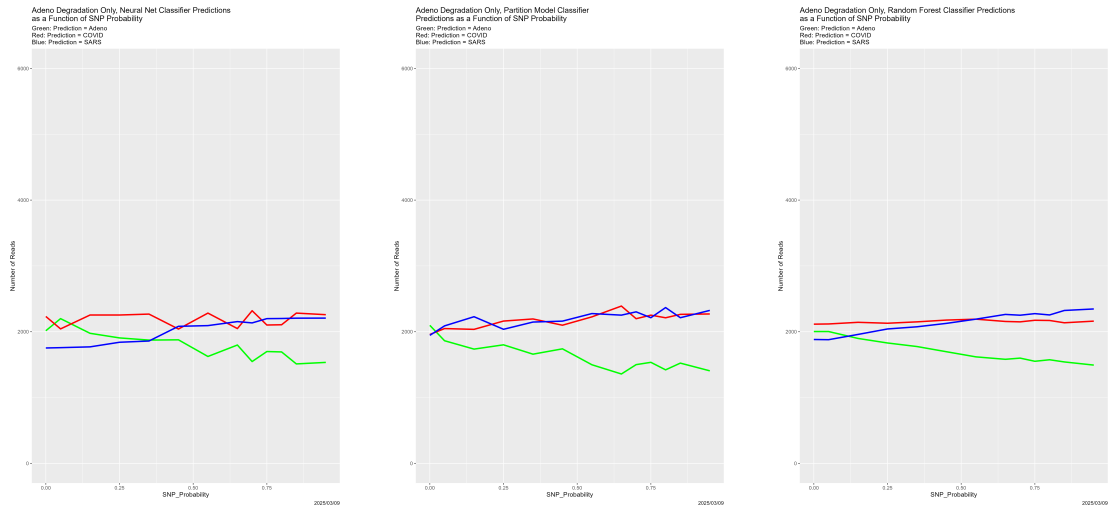


Figure 17: SNP degradation applied only to Adeno reads: classifier predictions as a function of SNP\_Probability. *Left:* neural net. *Center:* partition model. *Right:* random forest. *Green:* prediction = Adeno. *Red:* prediction = COVID. *Blue:* prediction = SARS.

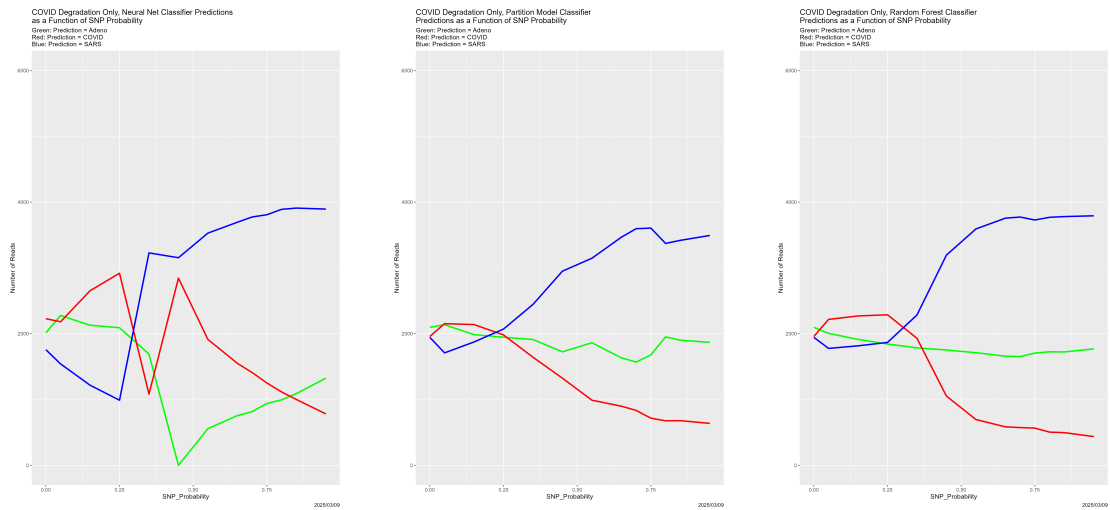


Figure 18: SNP degradation applied only to COVID reads: classifier predictions as a function of SNP\_Probability. *Left:* neural net. *Center:* partition model. *Right:* random forest. *Green:* prediction = Adeno. *Red:* prediction = COVID. *Blue:* prediction = SARS.

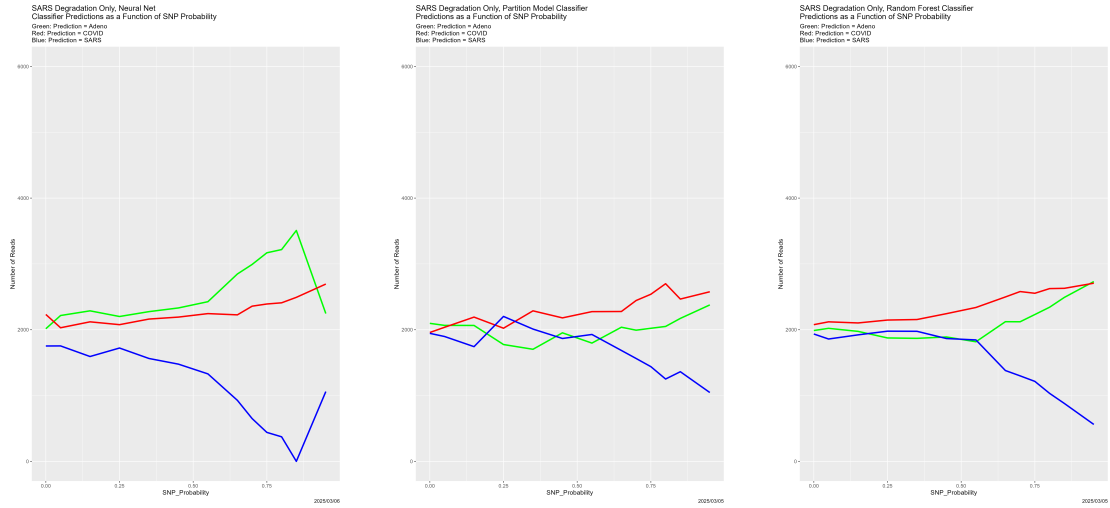


Figure 19: SNP degradation applied only to SARS reads: classifier predictions as a function of SNP\_Probability. *Left:* neural net. *Center:* partition model. *Right:* random forest. *Green:* prediction = Adeno. *Red:* prediction = COVID. *Blue:* prediction = SARS.

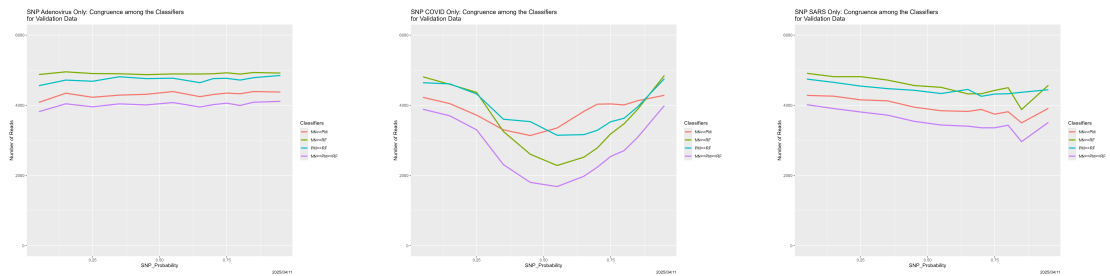


Figure 20: SNP degradation applied only to one set of reads: classifier congruence as a function of SNP\_Probability. *Left:* applied only to Adeno reads in training data. *Center:* applied only to COVID reads in training data. *Right:* applied only to SARS reads in training data.

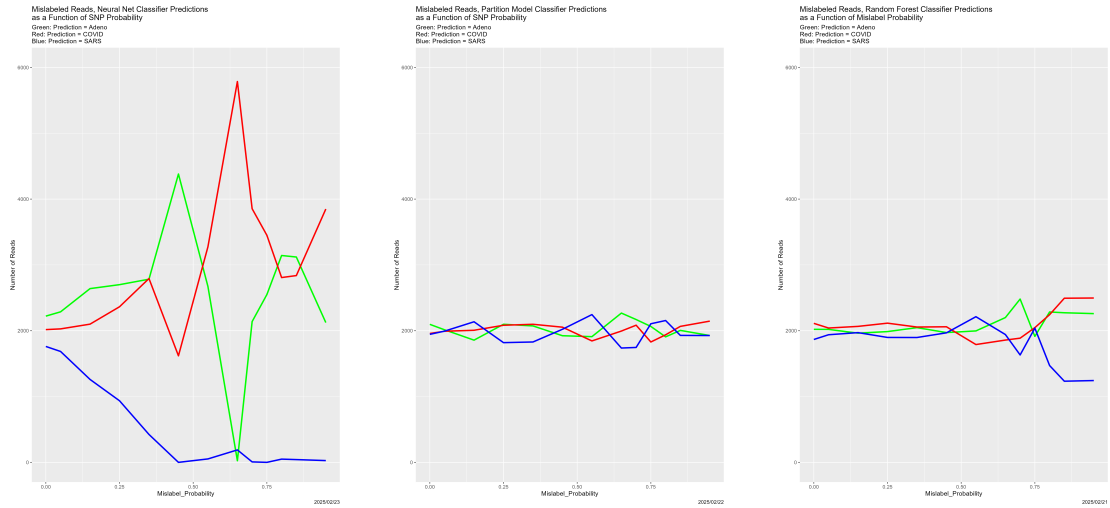


Figure 21: Mislabeled training data: classifier predictions as a function of Mislabel\_PROBABILITY. *Left:* neural net. *Center:* partition model. *Right:* random forest. *Green:* prediction = Adeno. *Red:* prediction = COVID. *Blue:* prediction = SARS.

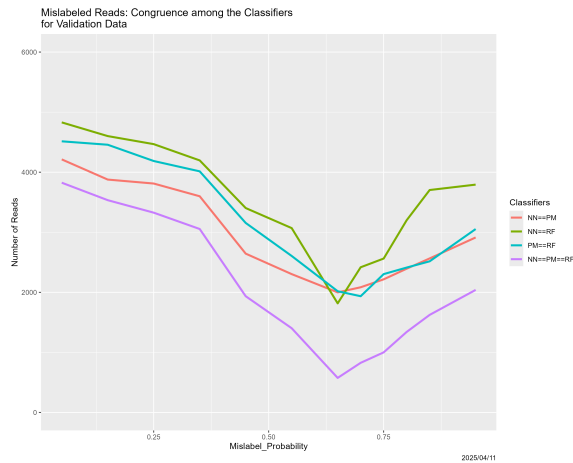


Figure 22: Mislabeled training data: classifier congruence as a function of Mislabel\_PROBABILITY.

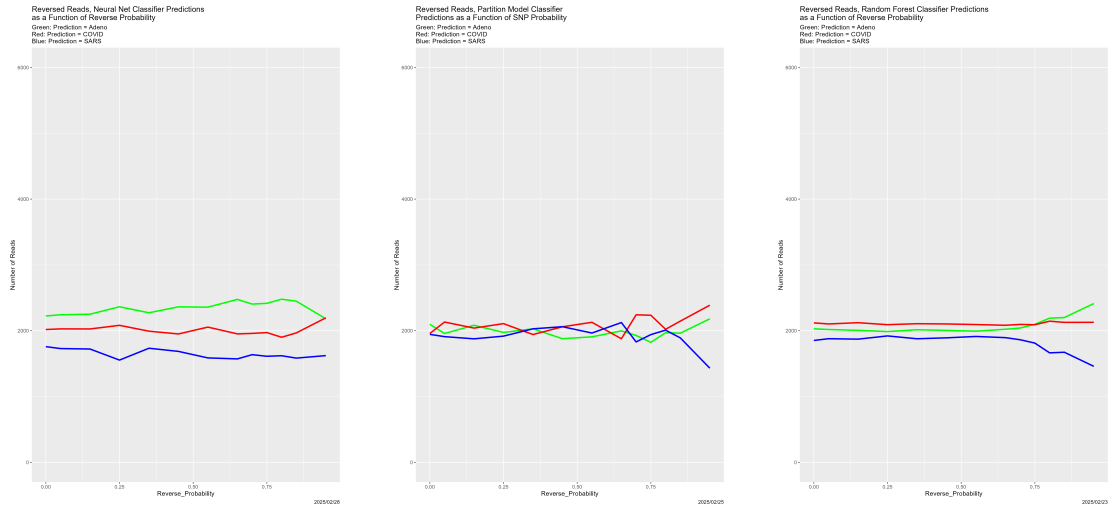


Figure 23: Reversed training data: classifier predictions as a function of the probability of reversing reads in the training dataset  $\mathcal{T}$ . *Left:* neural net. *Center:* partition model. *Right:* random forest. *Green:* prediction = Adeno. *Red:* prediction = COVID. *Blue:* prediction = SARS.

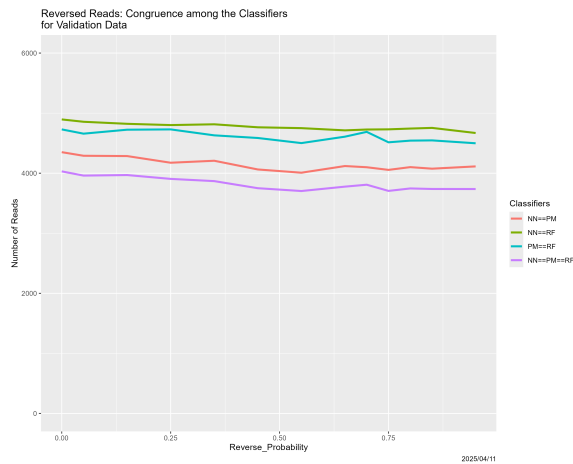


Figure 24: Reversed training data: classifier congruence as a function of probability of reversing reads in the training dataset  $\mathcal{T}$ .

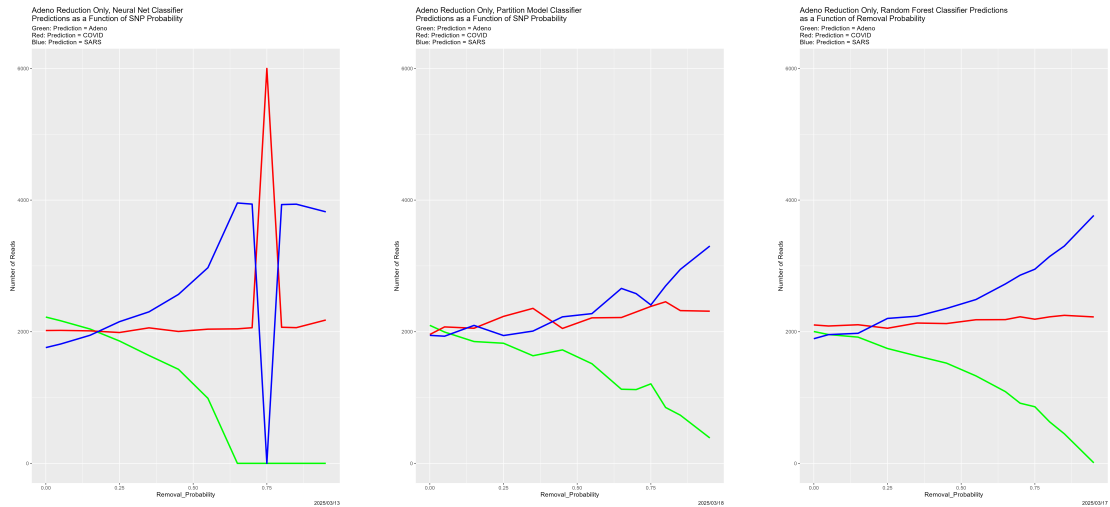


Figure 25: Reduced Adeno reads: classifier predictions as a function of Removal\_Probability. *Left:* neural net. *Center:* partition model. *Right:* random forest. *Green:* prediction = Adeno. *Red:* prediction = COVID. *Blue:* prediction = SARS.

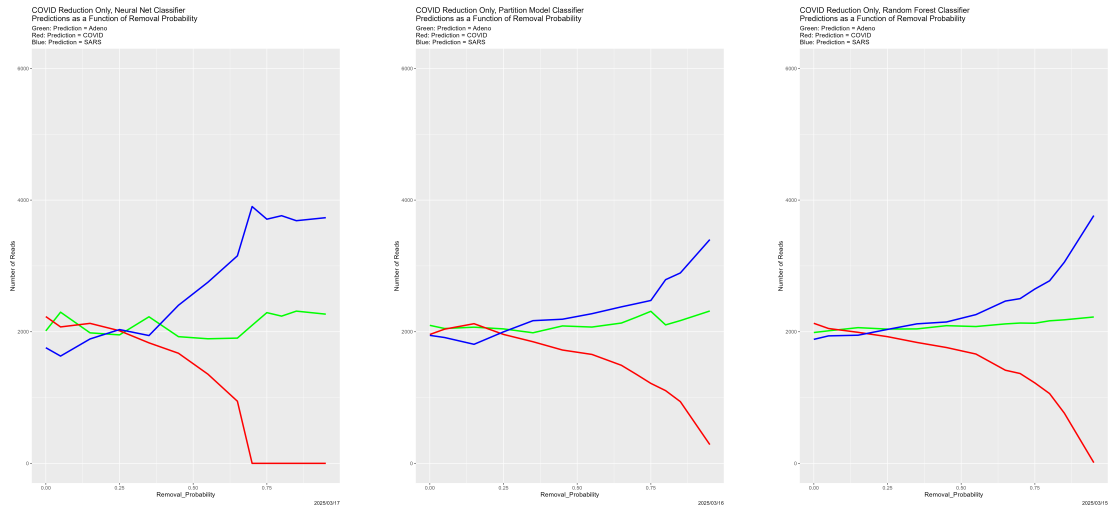


Figure 26: Reduced: COVID reads: classifier predictions as a function of Removal\_Probability. *Left:* neural net. *Center:* partition model. *Right:* random forest. *Green:* prediction = Adeno. *Red:* prediction = COVID. *Blue:* prediction = SARS.

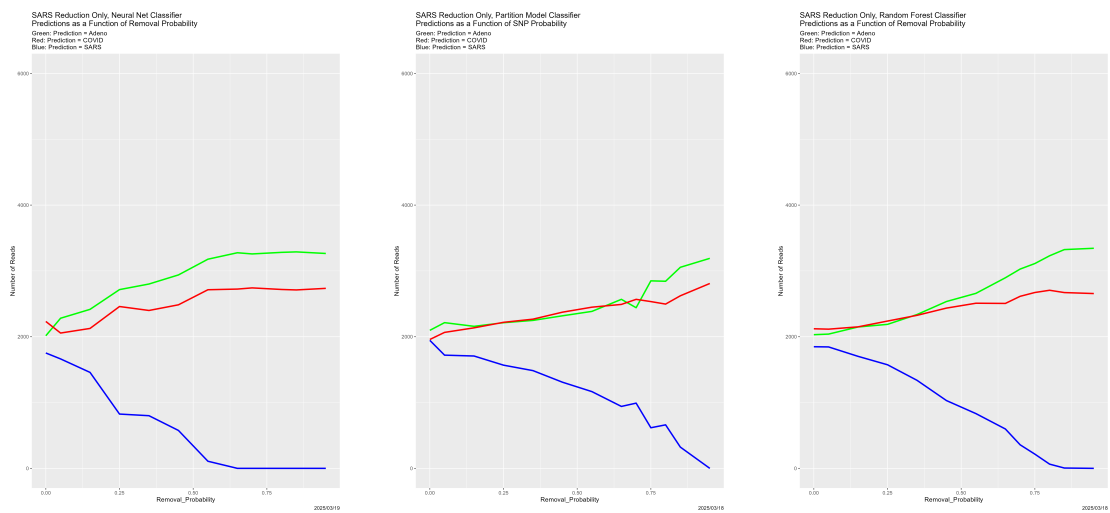


Figure 27: Reduced SARS reads: classifier predictions as a function of Removal\_Probability. *Left:* neural net. *Center:* partition model. *Right:* random forest. *Green:* prediction = Adeno. *Red:* prediction = COVID. *Blue:* prediction = SARS.

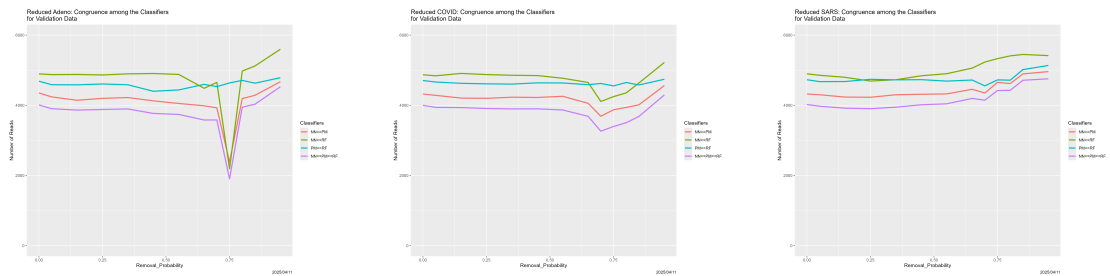


Figure 28: Reduced training data reads: classifier congruence as a function of Removal\_Probability. *Left:* reduced Adeno reads. *Center:* reduced COVID reads. *Right:* reduced SARS reads.

Add_Probability	Pred_Adeno	Pred_COVID	Pred_SARS	Pred_EColi	Pred_H5N1	Pred_HPVP	Pred_Norovirus	Pred_PGingivalis
0.000	2015	2232	1753	0	0	0	0	0
0.001	1945	2192	0	0	0	1863	0	0
0.005	279	2249	0	0	0	867	2605	0
0.010	0	2467	0	0	0	0	1335	2198
0.050	0	2873	0	0	0	0	2923	204
0.100	0	2610	0	0	0	0	3390	0
0.200	0	2027	0	0	0	0	3973	0

Add_Probability	Pred_Adeno	Pred_COVID	Pred_SARS	Pred_EColi	Pred_H5N1	Pred_HPVP	Pred_Norovirus	Pred_PGingivalis
0.000	2097	1958	1945	0	0	0	0	0
0.001	1864	2006	2023	0	0	0	0	107
0.005	1507	1986	1787	0	0	0	0	720
0.010	1081	2003	1708	0	0	0	0	1208
0.050	0	2098	707	0	0	0	0	3195
0.100	0	1653	450	0	0	0	0	3897
0.200	0	1459	0	0	0	0	0	4541
0.300	0	931	0	0	0	0	0	5069
0.400	0	788	0	0	0	0	0	5212
0.500	0	932	0	0	0	0	0	5068
0.600	0	0	0	0	0	0	0	6000
0.700	0	0	0	0	0	0	0	6000
0.800	0	0	0	0	0	0	0	6000

Add_Probability	Pred_Adeno	Pred_COVID	Pred_SARS	Pred_EColi	Pred_H5N1	Pred_HPVP	Pred_Norovirus	Pred_PGingivalis
0.000	2033	2119	1848	0	0	0	0	0
0.001	2024	2081	1889	0	0	0	0	6
0.005	1552	2110	1844	0	0	0	0	494
0.010	793	2173	1640	0	0	0	0	1394
0.050	0	1745	250	0	0	0	0	4005
0.100	3	972	0	0	0	0	0	5025
0.200	2	256	0	0	0	0	0	5742
0.300	1	0	0	0	0	0	0	5999
0.400	0	0	0	0	0	0	0	6000
0.500	3	0	0	0	0	0	0	5997
0.600	0	0	0	0	0	0	0	6000
0.700	0	0	0	0	0	0	0	6000
0.800	0	0	0	0	0	0	0	6000
0.900	0	0	0	0	0	0	0	6000
1.000	0	0	0	0	0	0	0	6000

Figure 29: Superfluous training data: classifier predictions as a function of Add\_Probability. *Top*: neural net. *Center*: partition model. *Bottom*: random forest.

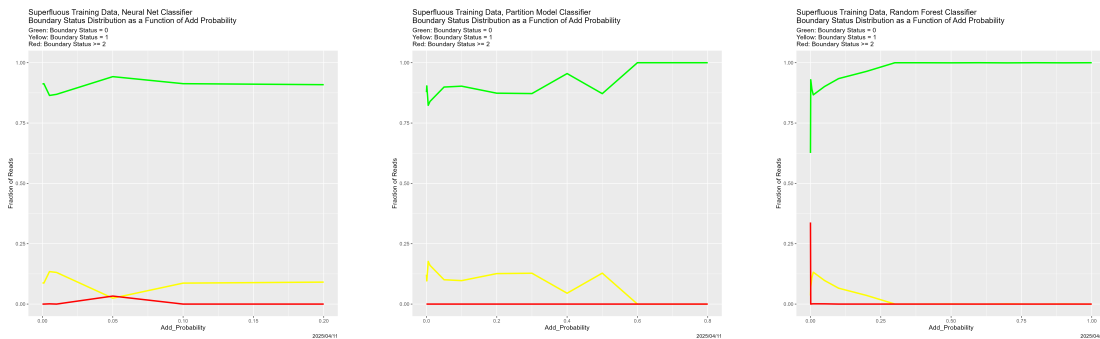


Figure 30: Superfluous training data: boundary status distributions as a function of Add\_Probability. In each of these, BS = 0 is the green line, BS = 1 is the yellow line, and BS = 2 is the red line.

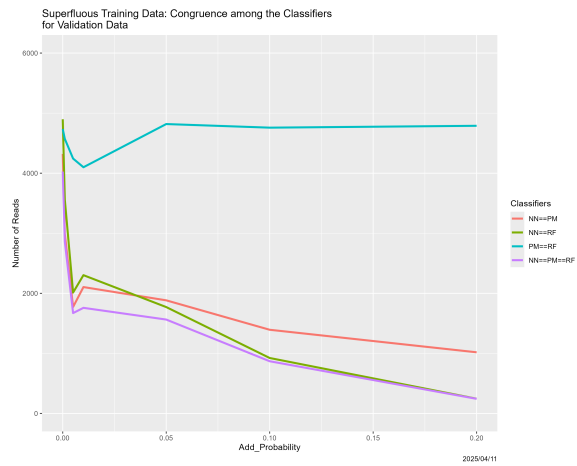


Figure 31: Superfluous training data: classifier congruence as a function of Add\_Probability.

## 5 Discussion

Despite its length, this paper leaves many questions unanswered.

### 5.1 Scientific Generalizability

We have examined one scientific context, with one input graph  $\mathcal{I}$  and one output space  $\mathcal{O}$ , four classifiers, and a handful of context-specific data quality characteristics. Of course, we have no evidence-based claim that what we have observed occurs more generally. We conjecture that it does, but asserting that breakdown is an inherent characteristic of classifiers, even those whose input space is a graph, let alone for all forms of data quality degradation, is simply silly. Nevertheless, our tools apply and our explanations make sense in virtually any context. And the world is full of discontinuities, including classifier boundaries, which are local discontinuities with respect to the analysis data, and are omnipresent.

Generalizability issues are of at least three varieties: with respect to scientific context/nature of datasets, classifiers, and data quality measures. In this paper we have addressed the latter two to some extent, but the first not at all. Doing so is most urgent question, and we plan to investigate it.

### 5.2 Theory vs. Empirical Evidence

We turn now to the question with which Section 4.1 ended “Why SNP\_Probability = 0.75?” Can there be theory that explains this? Given that our experiments are simulations in which we examined a limited set of possible values of SNP\_Probability, it seems sensible to believe that 0.75 is the mean (or another characteristic) of some random variable that varies depending on exactly which bases in which reads are altered. While the same breakdown phenomenon may exist in other settings, the numerical value is setting- and data quality measure-specific.

There may be a deeper issue here, which is the role of empirical analyses in understanding computational tools that lack theory capable of predicting their behavior in reality, especially for datasets sampled from non-describable population. To the extent that it is an issue for the classifiers here, it is a much more profound issue for large language models (LLMs) and other AI tools.

### 5.3 Actionable Implications

And now the really big question: so what? With slightly more precision, our high-level path to impact is that:

- Classifier performance depends on training data, which we have demonstrated in one context.
- In today’s world, many datasets are collected with limited attention to quality, and little-to-no characterization or quantification of it.
- The principled way to deal with these two phenomena is via uncertainties associated with classifier decisions, as measured by Neighbor Similarity, for instance. Doing so without changing the training data quality is not possible.

We also note that one of us (AFK) has argued that data quality is for aficionados, and that it is really decision quality that matters (Karr, 2013). To this end, combining this paper with findings in Karr et al.

(2026) and Porter and Karr (2024), what may be the central data quality issue emerges—beyond the quality of  $\mathcal{T}$  (addressed here) and that of  $\mathcal{V}$ , there is the quality of relationship between the training data and analysis data. “Everyone knows” that if they are too divergent, performance suffers. This paper and Karr et al. (2026) are steps to quantifying both the divergence and the performance consequences. Is there a paradigm, probably iterative and therefore necessarily Bayesian, that addresses the problem? For instance, start with a large training dataset  $\mathcal{T}$ , run the classifier(s) and see whether there are unused elements of  $\mathcal{T}$  that can be removed. Assess quality of elements  $\mathcal{T}$  to see if there are low quality elements whose removal would improve performance. Then, re-run the process. And at some point, assess whether there are elements of  $\mathcal{V}$  that may be misclassified because they are of low quality. The role of Bayes in such a paradigm is to track uncertainties properly.

## 6 Conclusion

In this paper, we have shown that in one context, decreasing the quality of data used to train classifiers impairs their performance, in some cases causing it to break down entirely. We have examined multiple mechanisms for effecting the quality decrease, which behave similarly. The consequences for decisions based on classifier output are beginning to be explored.

## Acknowledgements

Precursor research by AFK was supported in part by NIH grant 5R01AI100947–06, “Algorithms and Software for the Assembly of Metagenomic Data,” to the University of Maryland College Park (Mihai Pop, PI). He thanks Professor Pop for numerous insightful discussions.

Both authors gratefully acknowledge ongoing support and collaboration from Professor Adam Porter of the University of Maryland College Park. This paper flows directly from Karr et al. (2022), Porter and Karr (2024), and Karr et al. (2026), of which he is a co-author.

## Declarations

- Both authors contributed equally to the paper.
- The authors declare no conflicts of interest or competing interests.
- Data and R code for the analyses in this paper are available at <https://doi.org/TBD>.

## A Neighbor Similarity for SNP Degradation

See Section 4.1 for discussion.

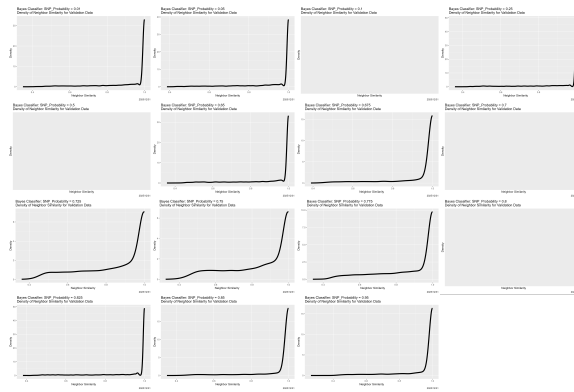


Figure 32: SNP degradation, Bayes classifier: Neighbor Similarity as a function of SNP\_Probability.

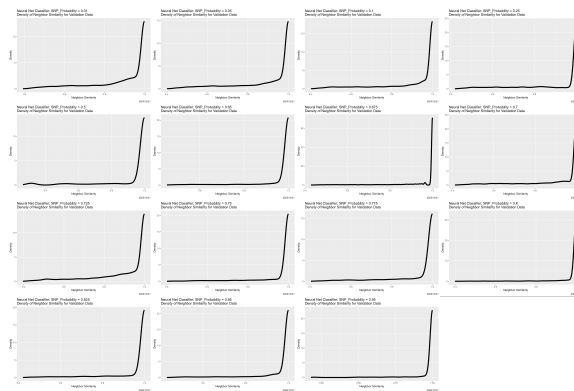


Figure 33: SNP degradation, neural net classifier: Neighbor Similarity as a function of SNP\_Probability.

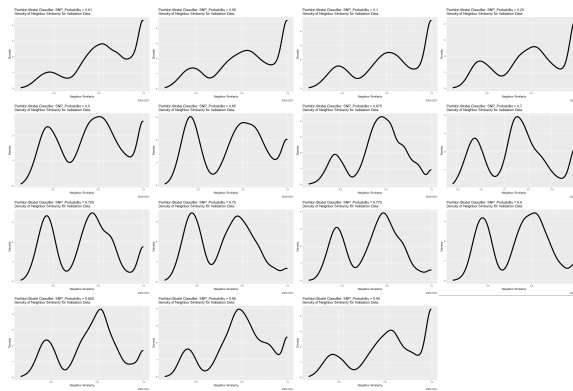


Figure 34: SNP degradation, partition model classifier: Neighbor Similarity as a function of SNP\_Probability.

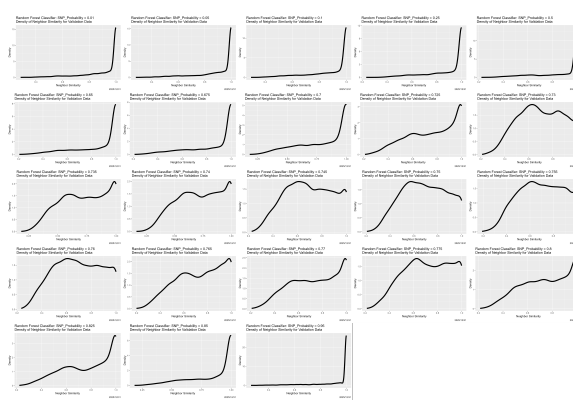


Figure 35: SNP degradation, random forest classifier: Neighbor Similarity as a function of SNP\_Probability.

## References

- Biemer, P. P., Leeuw, E. D., Eckman, S., Edwards, B., Kreuter, F., Lyberg, L., Tucker, C., and West, B., editors (2017). *Total Survey Error in Practice*. Wiley, New York.
- Cepeda, V., Liu, B., Almeida, M., Hill, C. M., Treangen, T. J., and Pop, M. (2017). MetaCompass: Reference-guided assembly of metagenomes. Preprint, bioRxiv, <https://doi.org/10.1101/212506>.
- Compeau, P. E. C., Pevzner, P. A., and Tesler, G. (2023). Why are de Bruijn graphs useful for genome assembly? *Nat. Biotechnol.*, 29(11):987–991.
- Farbiash, D. and Puzis, R. (2020). Cyberbiosecurity: DNA injection attack in synthetic biology. arXiv:2011.13444v1 [cs.CR].
- Fedorov, V. V. (1972). *Theory of Optimal Experiments*. Academic Press, New York.
- Hastie, T., Tibshirani, R., and Friedman, J. (2001). *The Elements of Statistical Learning: Data Mining, Inference, and Prediction*. Springer–Verlag, New York.
- Holtgrewe, M. (2010). Mason: A read simulator for second generation sequencing data. *Technical Report FU Berlin*.
- Karr, A. F. (2013). Discussion of five papers on “Systems and Architectures for High-Quality Statistics Production”. *Journal of Official Statistics*, 29(1):157–163.
- Karr, A. F. (2017). The role of statistical disclosure limitation in total survey error. In Biemer, P. P., Leeuw, E. D., Eckman, S., Edwards, B., Kreuter, F., Lyberg, L., Tucker, C., and West, B., editors, *Total Survey Error in Practice*, pages 71–94. Wiley, New York.
- Karr, A. F., Hauzel, J., Porter, A. A., and Schaefer, M. (2022). Measuring quality of DNA sequence data via degradation. *PLoS ONE*, 2022:0221459. DOI: 10.1371/journal.pone.0221459.
- Karr, A. F., Hauzel, J., Porter, A. A., and Schaefer, M. (2023). Application of Markov structure of genomes to outlier identification and read classification. Preprint. arXiv:2112.13117.
- Karr, A. F., Porter, A. A., Bowen, Z., and Ruane, R. (2026). Structure of classifier boundaries: Case study for a Bayes classifier. *J. Classification*. Under revision; arXiv:2212.04382.
- Karr, A. F., Sanil, A. P., and Banks, D. L. (2006). Data quality: A statistical perspective. *Statistical Methodology*, 3(2):137–173.
- Karr, A. F., Sanil, A. P., Sacks, J., and Elmagarmid, E. (2001). Workshop Report: Affiliates Workshop on Data Quality. Technical Report, National Institute of Statistical Sciences. Available online at [www.niss.org/affiliates/dqworkshop/report/dq-report.pdf](http://www.niss.org/affiliates/dqworkshop/report/dq-report.pdf).
- Keller, S., Korkmaz, G., Orr, M., Schroeder, A., and Shipp, S. (2017). The evolution of data quality: understanding the transdisciplinary origins of data quality concepts and approaches. *Annu. Rev. Stat. Appl.*, 4:85–108.

- Nikulin, M. S. (2001). Hellinger distance. In *Encyclopedia of Mathematics*. EMS Press, Berlin.
- Office of Management and Budget (2002). Guidelines for Ensuring and Maximizing the Quality, Objectivity, Utility, and Integrity of Information Disseminated by Federal Agencies. Available online at [www.whitehouse.gov/omb/fedreg/reproducible.html](http://www.whitehouse.gov/omb/fedreg/reproducible.html).
- Office of Management and Budget (2006). Standards and Guidelines for Statistical Surveys; Statistical Policy Directive No. 2. Downloaded on 9/2/2021 from <https://www.whitehouse.gov/omb/information-regulatory-affairs/statistical-programs-standards/>.
- Pop, M. (2024). MetaCompass: Comparative assembly of metagenomic sequences. Information available at <https://metacompass.cbcb.umd.edu/>.
- Porter, A. A. and Karr, A. F. (2024). Active model learning for software interrogation and diagnosis. ICSE 2024 Workshop on Advances in Model-Based Software Testing (A-MOST).
- Pride, D. T., Meinersmann, R. J., Wassenaar, T. M., and Blaser, M. J. (2003). Evolutionary implications of microbial genome tetranucleotide frequency biases. *Genome Research*, 13:145–158.
- Riedmiller, M. (1994). Rprop - Description and Implementation Details. Technical report, University of Karlsruhe.
- Teeling, H., Meyerdierks, A., Bauer, M., Amann, R., and Glöckner, F. O. (2004a). Application of tetranucleotide frequencies for the assignment of genomic fragments. *Environmental Microbiology*, 6(9):938–947.
- Teeling, H., Waldmann, J., Lombardot, T., Bauer, M., and Glöckner, F. O. (2004b). TETRA: a web-service and a stand-alone program for the analysis and comparison of tetranucleotide usage patterns in DNA sequences. *BMC Bioinformatics*, 5(163).
- Watson, J. D. (2001). *The Double Helix: A Personal Account of the Discovery of the Structure of DNA*. Touchstone, New York.
- Wheeler, R. E. (2004). *AlgDesign: Algorithmic Experimental Design*. R package.